

BUBBLE PUMP DESIGN AND PERFORMANCE

A Thesis
Presented to
The Academic Faculty

By

Susan Jennifer White

In Partial Fulfillment
of the Requirements for the Degree
Master of Science in Mechanical Engineering

Georgia Institute of Technology
August 2001

BUBBLE PUMP DESIGN AND PERFORMANCE

Approved:

S. V. Shelton, Chairman

S. M. Ghiaasiaan

S. M. Jeter

Date Approved _____

TABLE OF CONTENTS

LIST OF TABLES	v
LIST OF FIGURES.....	vi
NOMENCLATURE.....	viii
SUMMARY	xi
CHAPTER I: INTRODUCTION.....	1
Dual Pressure Absorption Cycles	2
Single Pressure Absorption Refrigeration	3
The Platen-Munters Cycle.....	4
The Einstein Cycle	6
CHAPTER II: LITERATURE REVIEW.....	8
Introduction	8
Einstein Cycle Bubble Pump.....	9
Platen-Munters Cycle Bubble Pump.....	9
Air-Lift Pumps	10
Two-Phase Flow.....	13
CHAPTER III: EXPERIMENTAL SETUP.....	16
Experimental Results	19
CHAPTER IV: MODEL.....	20
Governing Equations	20
Two-Phase Properties	25
The Drift Flux Model.....	27
Comparison of Models.....	34
CHAPTER V: RESULTS AND DISCUSSION.....	42
Air-Lift Pump Experiments	42
Parametric Studies.....	42
Optimum Operating Conditions	48
Slug - Churn Transition.....	51
Ammonia-Water Model.....	53

CHAPTER VI: CONCLUSIONS AND RECOMMENDATIONS.....	59
REFERENCES.....	62

LIST OF TABLES

Table 2.1: Two-Phase Flow Parameters	14
--	----

LIST OF FIGURES

Figure 1.1: Dual Pressure Absorption System	2
Figure 1.2: The Einstein Refrigeration Cycle	5
Figure 1.3: The Ammonia-Water-Hydrogen Cycle	7
Figure 2.1: Bubble Pump Configuration	11
Figure 2.2: Vertical Two-Phase Flow Regimes	15
Figure 3.1: Experimental Setup	18
Figure 4.1: Air Flow Rate vs. Liquid Mass Flow Rate ($\alpha = 0.4$, $D = 6\text{mm}$).....	35
Figure 4.2: Air Flow Rate vs. Liquid Mass Flow Rate ($\alpha = 0.4$, $D = 8\text{mm}$)	35
Figure 4.3: Air Flow Rate vs. Liquid Mass Flow Rate ($\alpha = 0.4$, $D = 10\text{mm}$)	36
Figure 4.4: Air Flow Rate vs. Liquid Mass Flow Rate ($\alpha = 0.6$, $D = 6\text{mm}$).....	36
Figure 4.5: Air Flow Rate vs. Liquid Mass Flow Rate ($\alpha = 0.6$, $D = 8\text{mm}$)	37
Figure 4.6: Air Flow Rate vs. Liquid Mass Flow Rate ($\alpha = 0.6$, $D = 10\text{mm}$)	37
Figure 4.7: Air Flow Rate vs. Liquid Mass Flow Rate ($\alpha = 0.8$, $D = 6\text{mm}$)	38
Figure 4.8: Air Flow Rate vs. Liquid Mass Flow Rate ($\alpha = 0.8$, $D = 8\text{mm}$)	38
Figure 4.9: Air Flow Rate vs. Liquid Mass Flow Rate ($\alpha = 0.8$, $D = 10\text{mm}$).....	39
Figure 5.1: Theoretical Efficiency vs. Liquid Mass Flow Rate ($\alpha = 0.4$)	43
Figure 5.2: Experimental Efficiency vs. Liquid Mass Flow Rate ($\alpha = 0.4$)	43
Figure 5.3: Theoretical Efficiency vs. Liquid Mass Flow Rate ($\alpha = 0.6$)	44

Figure 5.4: Experimental Efficiency vs. Liquid Mass Flow Rate ($\alpha = 0.6$)	44
Figure 5.5: Theoretical Efficiency vs. Liquid Mass Flow Rate ($\alpha = 0.8$).....	45
Figure 5.6: Experimental Efficiency vs. Liquid Mass Flow Rate ($\alpha = 0.8$)	45
Figure 5.7: Length Effect: Experimental Air Flow Rate vs. Liquid Mass Flow Rate ($\alpha = 0.4$, $D = 6\text{mm}$)	47
Figure 5.8: Length Effect: Theoretical Air Flow Rate vs. Liquid Mass Flow Rate ($\alpha = 0.4$, $D = 6\text{ mm}$)	47
Figure 5.9: Efficiency vs. Liquid Mass Flow Rate ($\alpha = 0.4$, $D = 8\text{ mm}$)	49
Figure 5.10: Air Flow Rate vs. Liquid Mass Flow Rate ($\alpha = 0.4$, $D = 8\text{ mm}$)	49
Figure 5.11: Flow Regime Map, $D = 6\text{ mm}$	50
Figure 5.12: Flow Regime Map, $D = 8\text{ mm}$	50
Figure 5.13: Flow Regime Map, $D = 10\text{ mm}$	50
Figure 5.14: Efficiency vs. Diameter ($\alpha = 0.4$)	55
Figure 5.15: Efficiency vs. Diameter ($\alpha = 0.6$)	56
Figure 5.16: Efficiency vs. Diameter ($\alpha = 0.8$)	56
Figure 5.17: Optimum Efficiency Diameter vs. Liquid Mass Flow Rate	57

NOMENCLATURE

Symbols

A	Cross-sectional area (m^2)
A_1	Constant
Bo	Bond Number
B_1	Constant
C	Constant (with subscripts 1-8)
C_o	Distribution parameter
C_n	Constants in Chexal-Lellouche Void Model ($n = 1, 2, \dots, 8$)
COP	Coefficient of Performance
D	Diameter of lift tube (m)
D_o	Diameter of entrance tube (m)
D_2	Reference diameter (m)
f	Friction factor
f'	Fanning friction factor
g	Acceleration of gravity (m/s^2)
H	Height of Generator liquid level (m)
j	Superficial velocity (m/s)
K	Experimental friction relationship
K_o	Correlating fitting parameter

L	Length of lift tube (m)
L_o	Length of entrance tube (m)
L_C	Chexal-Lellouche fluid parameter
m	Constant (different drift flux analysis than in slug/churn transition analysis)
\dot{m}	Mass flow rate (kg/s)
n	Constant
N_f	Viscous effects parameter
P	Pressure (bars)
Q	Volumetric flow rate (m ³ /s)
\dot{Q}	Heat transfer rate (W)
r	Correlating fitting parameter
Re	Reynolds number
S	Slip between phases of two-phase flow
T	Temperature (K)
V	Velocity (m/s)
x	Quality
Y	Mole fractions

Greek characters

ε	Void fraction
ε_R	Pipe roughness (m)
ρ	Density (kg/m ³)

μ	Fluid viscosity (kg/m-s)
σ	Surface tension (N/m)
Σ	Surface tension number
\dot{V}	Volumetric Flow Rate (m ³ /s)

Subscripts

0	State 0 (in governing equations)
1	State 1 (in governing equations)
2	State 2 (in governing equations)
a	Ammonia
BP	Bubble pump
G	Gas
gj	Drift
h	Homogeneous conditions (in two-phase flow)
L	Liquid
m	Mixture
TP	Two-phase
v	Vertical
w	Water

Superscripts

*	non-dimensionalized
---	---------------------

SUMMARY

Contrary to conventional dual and triple pressure absorption refrigeration cycles, a single pressure absorption cycle does not require mechanical work to pump fluid from the absorber to the higher-pressure generator. However, the single pressure cycle does require a mechanism to lift the fluid from the generator to the absorber against gravity and friction. A bubble pump, or vapor-lift pump, is used for this task because it requires only thermal energy input as the driving force, which is the same as that required to drive the absorption cycle.

In a bubble pump, heat addition creates vapor, thereby increasing the buoyancy of the fluid causing it to rise through a vertical tube under two-phase flow conditions. Air-lift pumps have been used for decades in the oil industry that run on the same principles, however instead of bubbles forming from the phase change involved with boiling the liquid, air is injected into the flow, creating the same buoyancy effect.

While two-phase vertical flow and air-lift pumps have been studied since the early part of the last century, no references studying the design optimization of a bubble pump are found in the open literature. In this paper, experimental studies are performed while different existing two-phase flow models' results are compared to the experimental data. The best-suited model is used to carry out parametric studies and to optimize for maximum efficiency under various operating conditions. Optimum efficiency is defined

as the liquid pumped per unit of bubble pump heat input. The results show there is an optimum bubble pump tube diameter for a given set of operating conditions.

The results are discussed and conclusions drawn regarding designing a bubble pump for a single pressure absorption cycle that will lift the required liquid fluid flow rate with the minimum bubble pump thermal input.

CHAPTER I

INTRODUCTION

Conventional vapor compression and absorption refrigeration systems are dual pressure cycles where the saturation temperature difference between the condenser and evaporator is produced by a system pressure difference. This requires a mechanical input to drive the compressor or pump needed to generate this change in pressure, which adds significantly to the noise level and cost of the system while reducing the reliability and portability. On the other hand single pressure absorption refrigeration systems, such as the Platen and Munters (1928) diffusion-absorption cycle and the Einstein cycle (1928), use at least three working fluids to create temperature changes by imposing partial pressures on the refrigerant. While termed “single pressure” there are still slight overall pressure variations within these cycles due to flow friction and gravity. So, despite there being no need to pump the fluid to a much higher pressure to create a change in saturation temperature, a mechanism is needed to move the fluid through the cycle against flow friction and gravity. To eliminate the need for a mechanical input, a heat-driven bubble pump is used for this purpose. In this study, the bubble pump component is analyzed so that design for optimum performance can be achieved.

Dual Pressure Absorption Cycles

In a dual pressure absorption system, the refrigerant circulates through the condenser, the expansion valve, and evaporator in much the same way as in a vapor-compression system (Figure 1.1). However, an absorption-generation process replaces the compressor. Now, instead of compressing a vapor between the evaporator and the condenser as in a vapor compression refrigeration cycle, the refrigerant is absorbed by a secondary substance, called an absorbent, to form a liquid solution. The liquid solution is then pumped to the higher pressure.

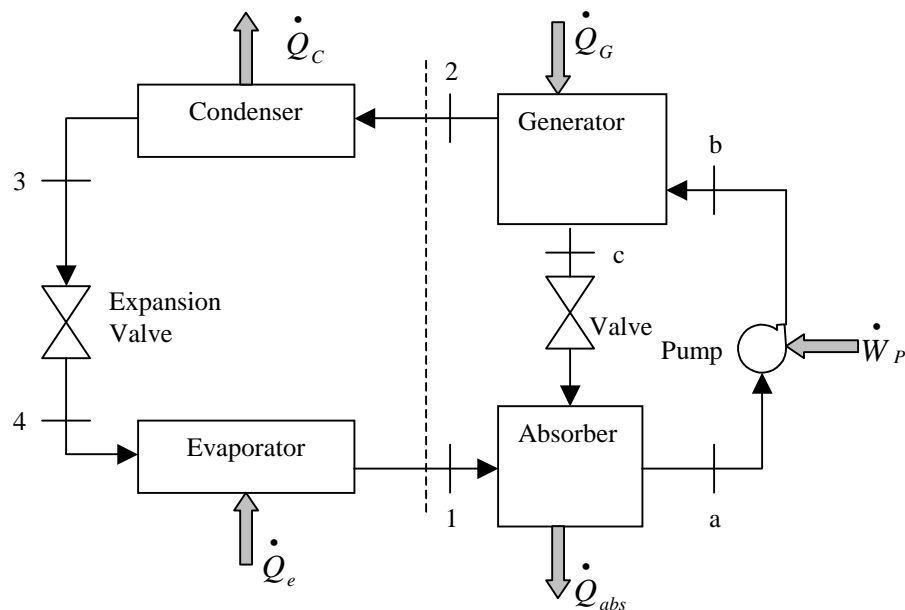


Figure 1.1: Dual Pressure Absorption System (Moran & Shapiro 1996)

Because the average specific volume of the liquid solution is much less than that of the refrigerant vapor, significantly less work is required than in a vapor compression cycle. Accordingly, absorption refrigeration systems have the advantage of relatively small work input compared to vapor-compression systems (Moran & Shapiro, 1996).

A generator is needed in the absorption cycle to separate the refrigerant vapor from the liquid solution before the refrigerant enters the condenser. This involves heat transfer from a relatively high-temperature source. The refrigerant then flows to the condenser, while the absorbent is throttled back to the lower pressure as it falls to the absorber.

Single Pressure Absorption Refrigeration

Two single pressure absorption refrigeration cycles are the Einstein Cycle (Einstein & Szilard 1928) and Platen and Munters' diffusion absorption cycle (von Platen & Munters 1928). Because of their single pressure operation, they are able to completely avoid the need for electric power, along with its associated central power plant and electric distribution infrastructure, and instead rely on a direct thermal energy source. This helps avert the need to wastefully convert heat to work and then back to heat. They also use environmentally benign fluids, an increasingly important issue as several man-made refrigerants are phased out over the next few years. Additionally, they are portable, reliable, operate silently, and are inexpensive to build. However, with relatively low refrigeration COP's, they have limited applications. When used for heating, both cycles can achieve efficiencies over 100% (Schaefer, 2000). In this situation, when competing against direct fired heating devices, the low COP is less of an issue.

The Platen-Munters Cycle

The Platen-Munters (1928) cycle is similar to a dual-pressure ammonia-water absorption cycle with an inert gas, usually hydrogen, diffused through the system to maintain a uniform system pressure throughout the cycle. Shown in Figure 1.2, the diffusion-absorption cycle consists of a generator, bubble pump, absorber, and condenser with ammonia, water, and hydrogen as the working fluids.

When heat is supplied to the generator (5), bubbles of ammonia gas are produced from the ammonia-water mixture. The ammonia bubbles rise and lift with them the weak ammonia-water solution, (weak in ammonia), through the bubble pump lift tube. The weak solution is sent to the absorber (6), while the ammonia vapor rises to the condenser (1). In the condenser, heat is removed from the ammonia vapor causing it to condense to a liquid at the system's total pressure. The condensed ammonia flows down into the evaporator (2). Hydrogen supplied to the evaporator passes across the surface of the ammonia, lowering the partial pressure on the liquid ammonia. This reduction in the partial pressure allows the liquid ammonia to evaporate at a lower temperature. The evaporation of the ammonia extracts heat from the evaporator, providing refrigeration to the desired space. The mixture of ammonia and hydrogen vapor falls from the evaporator to the absorber (3). A continuous trickle of weak ammonia-water solution enters the upper portion of the absorber (6). It is fed by gravity from the bubble pump. This weak ammonia-water solution absorbs the vapor ammonia leaving the light hydrogen to rise back to the evaporator (4). Finally, the strong ammonia-water solution flows back into the generator/bubble pump system (5), thus completing the cycle.

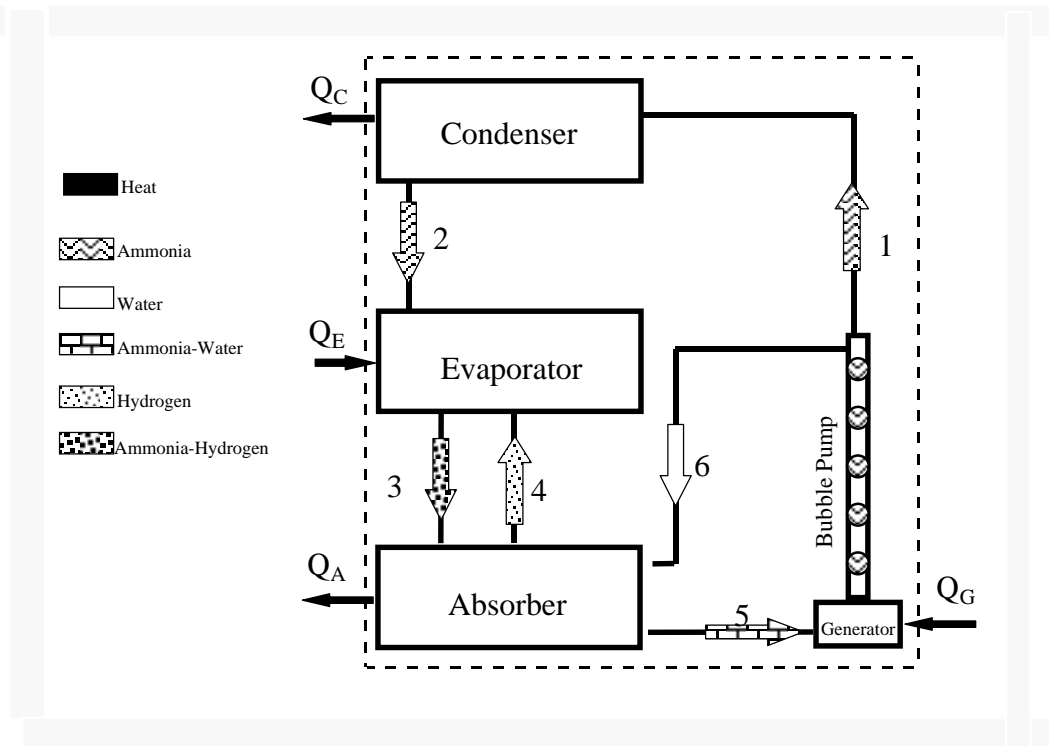


Figure 1.2: Diffusion-Absorption Cycle

The diffusion-absorption cycle has a niche market in the recreational vehicle and hotel room refrigerator markets (Herold et. al. 1996). It is manufactured in many parts of the world today. These units have a COP of approximately 0.15 to 0.2. Since its invention several attempts have been made to make it more competitive with dual-pressure cycles by improving its efficiency, but at refrigeration temperatures a COP of approximately 0.3 is the best published efficiency (Chen et. al. 1996).

The Einstein Cycle

In 1928 Einstein and Szilard also patented a single pressure absorption cycle. Delano (1998) performed a design analysis of the cycle and added two regenerative heat exchangers to improve efficiency. These include an internal regenerative heat exchanger in the generator and an evaporator pre-cooler. His cycle schematic can be seen in Figure 1.3.

Unlike the Platen-Munters cycle, the Einstein cycle uses a pressure-equalizing absorbate fluid rather than an inert gas. In the Einstein cycle, butane is the refrigerant, water remains the absorbent, and ammonia becomes the pressure-equalizing fluid. The generator, bubble pump, and evaporator are the same as the Platen-Munters cycle, but the condenser and absorber are combined into a single unit. It also operates as a single pressure system. In the evaporator, the partial pressure on the entering liquid butane is reduced by ammonia vapor, allowing it to evaporate at a lower temperature. In the condenser/absorber, the partial pressure of the butane vapor coming from the evaporator is increased when the ammonia vapor is absorbed by liquid water, thus allowing the butane to condense at a higher temperature. The liquid butane and liquid ammonia-water naturally separate due to their respective density differences and the fact that ammonia-water is immiscible with butane at the condenser/absorber's temperature and pressure. The ammonia is then separated from the water in a generator by the application of heat.

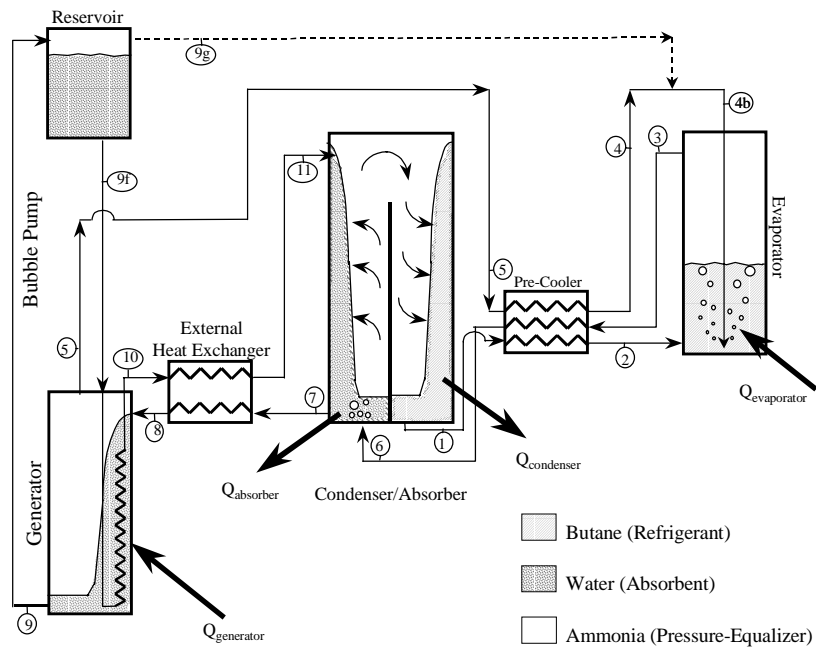


Figure 1.3: The Einstein Refrigeration Cycle

While early models predicted the cycle's cooling COP to be about 0.4, more recent studies have shown it to be about 0.2 (Shelton, et. al. 1999), which is relatively low compared to the thermal efficiency of dual pressure refrigeration cycles, but competitive with the diffusion-absorption cycle. One advantage of the Einstein cycle is its use of a different generator absorbate, ammonia, than that used in the evaporator, butane. This decouples the temperature difference between the generator/condenser and the condenser/evaporator allowing more flexibility in cycle design.

CHAPTER II

LITERATURE REVIEW

Introduction

Information on bubble pumps, also known as vapor-lift pumps, is sparse in the open literature. Percolating coffee makers are a well-known application of bubble pumps. Heat addition to the fluid at the base of a vertical tube creates vapor, thereby increasing the buoyancy of the fluid causing it to rise through the vertical tube under two-phase flow conditions, as seen in figure 2.1. Only the work of one author (Delano 1998) has addressed the design of a bubble pump for use in a single pressure absorption refrigeration cycle, with others (Schaeffer 2000, Sathe 2001) referencing this model.

Air-lift pumps are very similar to vapor-lift pumps, with a different mechanism to increase the buoyancy of the fluid. There is much more information available in the open literature on air-lift pumps. Most are based on the assumption of two-phase slug flow. Additionally, few have the same range of lift (~0.5 to 1 m) and diameters (~6 to 10 mm) that are applicable to the current study. Both air and vapor-lift pumps, however, are simply two-phase flow in a vertical tube; therefore two-phase flow models can be used to analyze the system.

Einstein Cycle Bubble Pump

Delano (1998) designed a model, based on the air-lift pump analysis of Stenning and Martin (1968), and analyzed the performance of the bubble pump of the Einstein cycle. It uses momentum balances and assigns a value recommended by Stenning and Martin (1968) for the slip ($S=V_G/V_L$) between phase velocities to model the two-phases involved. Schaefer (2000) used Delano's (1998) model with a turbulent single-phase friction factor instead of an experimentally determined one. In addition, Schaeffer analyzed the relationship of diameter, submergence ratio, mass flow rate, and heat input to maximize performance.

Platen-Munters Cycle Bubble Pump

Recently there has been a lot of interest in the Platen and Munters cycle. Herold et. al (1996) gives a review of the details of its operation and performance. Chen et. al (1996) investigated the diffusion-absorption cycle for enhancing its performance. The result was a new design for the bubble pump/generator configuration. The original design combines the generator and the bubble pump into one component, with only one heat addition. The modified version heats the strong ammonia solution first, extracting most of the ammonia from the water so that a weak ammonia solution is sent to the bubble pump where another heater causes the solution to boil and rise, due to increased buoyancy, through the lift tube. This design is virtually identical to the bubble pump/generator configuration in the Einstein cycle; therefore the same bubble pump model can be used for both cycles.

Chen et al (1996) experimentally found that this new configuration increased the cycle COP by about 50%, however a detailed theoretical model was not developed in this publication. Earlier, Hassoon (1991) provided a theoretical model and experimental results for a bubble pump that used injected steam for lift instead of vaporizing the liquid in the tube. However, it modeled a lift tube that was cooled along its length. Its application was for an ammonia-water absorption heat pump. More recently, Sathe (2001) used Delano's (1998) methodology applied to the Platen-Munters' bubble pump.

Air-Lift Pumps

Air-Lift pumps run on the same principals as vapor-lift pumps except that air is injected to increase the buoyancy of the fluid instead of bubbles forming from liquid vaporization. Although air-lift pumps have a wide variety of possible applications, most studies have been concerned with dewatering mines or raising oil from dead wells. More recently, the importance of air lifts in moving liquids at nuclear fuel reprocessing plants has been realized, requiring more accurate design equations (Clark and Dabolt 1986).

There is a large amount of literature on air-lift pumps, and since their operation is similar to that of bubble pumps, the analyses of them can be readily applied to bubble pumps. Stepanoff (1929) used a thermodynamic approach to investigate air-lift pumps and was able to physically describe their performance but offered no empirical data to back up the analysis. Pickert (1932) analyzed the performance of air-lift pumps, but as with many other studies, this was prior to the development of two-phase flow theory.

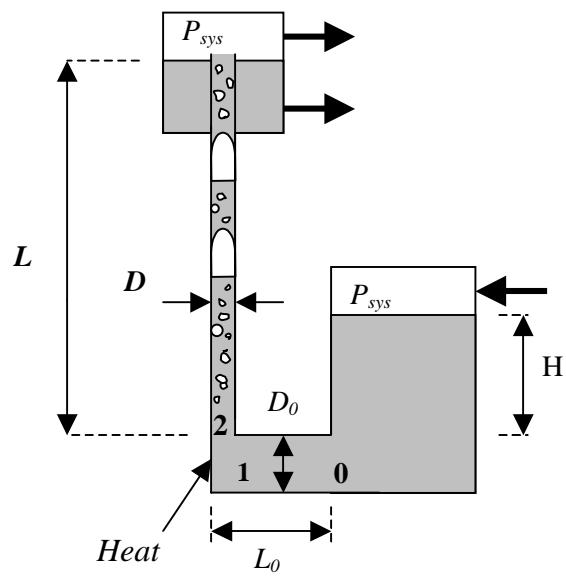


Figure 2.1: Bubble Pump Configuration

It must also be mentioned that most of these publications refer to generally large lift tubes, diameters 25-300 mm and lengths 10-200 m, well out of the range of the current study. However, Nicklin (1963) speculated that increased efficiency might be obtained by using small-diameter tubes at low flow rates, realizing along with White & Beardmore (1962) and Zukoski (1966) that as the tube diameter is decreased below 20 mm, the effects of surface tension on the dynamics of vertical slug flow become increasingly important.

With recent progress during the second half of the last century in understanding two-phase flows, Stenning and Martin (1968) introduced the basic principles of two-phase flow and momentum for investigating relatively small diameter and low lift air-lift pumps. Stenning and Martin's (1968) model is the starting point for Delano's (1998) analysis of the bubble pump. A study of the performance of the air-lift pump is carried out in the Stenning and Martin study. Liquid water volume flow rate (Q_L) is plotted versus air volume flow rate (Q_G) for various submergence ratios (H/L). It was determined that there is an airflow rate which produces a maximum water flow rate for a given tube diameter. Delano (1998) produces the same plots in his study, and defines his bubble pump to operate at this maximum water flow rate.

Lately, Kouremenos and Staicos (1985) carried out their investigations on small diameter air-lift pumps down to 12 mm diameters and low lift in the range of 1 to 3 m, with submergence ratios between 0.55 and 0.7. In the current study, the lift tube diameters considered are slightly smaller than this, with a larger range of submergence ratios. Also, Kouremenos and Staicos devised their experiments to obtain "perfect" slug

flow. For the current study, the flow regime was originally not constrained, however after performing experiments it was found that the most efficient flow regime was in fact slug flow.

Clark and Dabolt (1986) published a model to predict the height to which an air-lift pump operating in the slug flow regime can lift a given volumetric flow rate of liquid, given the air flow rate and the pressure at the point of gas introduction. The focus of this study was on accurately designing very tall air-lifts for nuclear fuel reprocessing, but it did not attempt an accurate description of the frictional pressure losses in the lift tube, and used an approximation of the general Lockhart-Martinelli (1949) correlation (de Cachard & Delhaye 1996).

More recent studies investigating the application of air-lift pumps in nuclear fuel reprocessing, such as de Cachard and Delhaye (1996), have been mostly interested in the accuracy of the air-lift pump model rather than with the efficiency. The extent to which they explore the two-phase fluid flow details around Taylor bubbles in the lift tube to obtain the frictional pressure drop is beyond the scope of this study. Certain assumptions have been made here to simplify the model considerably, without risking much degradation in accuracy due to the small scale of the bubble pump to be used.

Two-Phase Flow

A bubble pump (air-lift or vapor-lift) is essentially just two-phase flow in a vertical pipe, which has been studied extensively, but not with a bubble pump design perspective. Chisholm (1983) provides a good starting point for basic definitions and flow patterns encountered in vertical pipe flows, but does not discuss design

optimization. Some of the terminology associated with two-phase flow is listed in Table

2.1:

Table 2.1: Two-Phase Flow Parameters

Parameter	Units (SI)	Definition
ρ_G	kg/m ³	Density of gas phase
ρ_L	kg/m ³	Density of liquid phase
D	m	Diameter of lift tube
$A=\pi D^2/4$	m ²	Total cross sectional area of pipe
A_G	m ²	Cross sectional area gas occupies
$A_L=A-A_G$	m ²	Cross sectional area liquid occupies
$\varepsilon = A_G/A$	-	Gas void fraction of the flow
\dot{V}_G	m ³ /s	Gas volumetric flow rate
\dot{V}_L	m ³ /s	Liquid volumetric flow rate
$\dot{V} = \dot{V}_L + \dot{V}_G$	m ³ /s	Total volumetric flow rate
$j_G = \dot{V}_G / A$	m/s	Gas superficial velocity
$j_L = \dot{V}_L / A$	m/s	Liquid superficial velocity
$j = j_L + j_G$	m/s	Total average velocity of flow
$V_G = j_G / \varepsilon$	m/s	Velocity of the gas
$V_L = j_L / (1 - \varepsilon)$	m/s	Velocity of the liquid
\dot{m}_G	kg/s	Mass flow rate of gas
\dot{m}	kg/s	Total mass flow rate
$x = \dot{m}_G / \dot{m}$	-	Quality
$S = V_G / V_L$	-	Slip between phases

In essence, two-phase flow is a mixture of either a vapor and a liquid or a gas and a liquid moving through a pipe. The four basic flow patterns observed in vertical two-phase flows are bubbly, slug, churn, and annular, are shown in Figure 2.2 (Collier and Thome 1996). However, the exact definitions of each vary by author and flows are sometimes described as a combination of patterns.

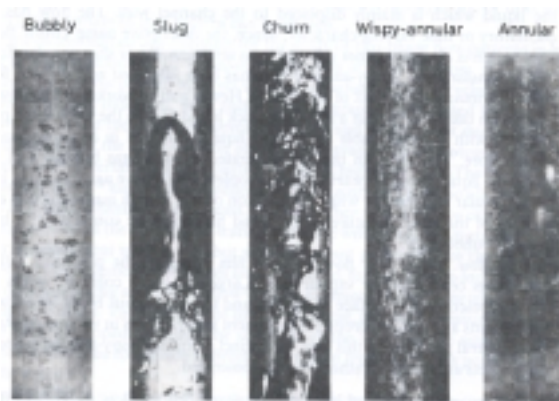


Figure 2.2: Vertical Two-Phase Flow Regimes (Collier & Thome 1996)

CHAPTER III

EXPERIMENTAL SETUP

Since airlift pumps operate in a similar manner as bubble pumps, an airlift pump has been used for the experimental analysis of the system due to the ease of its setup. The model is the same for an air-water system as an ammonia-water one, except for the fluid properties and the small changes in conservation of mass associated with the addition of air instead of boiling to create vapor.

Two experimental setups were built, one with a lift tube length of 3 ft and the other 6 ft, to establish length effect. The two setups have identical components other than the length of the tubes. The 3 ft experiment is described here in detail.

A picture of the 3 ft experimental setup is shown in Figure 3.1. Poly Vinyl Chloride (PVC) pipes, of 1.5 in. inner diameter, were used for construction of the reservoirs. The lift tubes used were clear and made of Pyrex with inner diameters of 6, 8, and 10 mm. The overall length was 36 in. Clear flexible Vinyl tubing of 0.25 in. inner diameter was used for connections with the liquid flow meter, while 0.125 in. tubing was used for air connections between the air pump, air flow meter, and for injection into the lift tube. An aerated end piece (a bubble diffuser used in fish tanks) was placed on the tip of the air injection tube to disperse the bubbles. Brass pipefittings were used to connect between the PVC and the flexible tubing, as well as between the flow meters and the

flexible tubing. A view tube made of the 0.125 in. flexible tubing was placed on the side of the holding reservoir so that an accurate reading of the liquid level could be made.

The water level in the reservoir on the right hand side of Figure 3.1 and the reservoir at the top of the lift tube were left open to the atmosphere, therefore $P_{\text{sys}} = 1\text{bar}$. The temperature of the system was atmospheric as well, $T=298\text{ K}$.

The air flow meter was an Omega FL-112 Rotameter, while the liquid flow meter was an Omega FL-114 Rotameter. Both flow meters have an accuracy of $\pm 2\%$ of the full scale. The meters had scales from 0 to 100 % that were dependent on the float material (glass was used in both). The ranges of values for the water flow meter were 0.1 to 15 gal/hour, while they were 0.004 to 2.3 L/min for the air flow meter. Valves were used to control the flow through the meters. Because of this, high liquid flow rates were not accurately measurable at a submergence ratio of 0.8 because the distance between the tube outlet and the fluid level in the reservoir did not provide a large enough pressure head to overcome the friction in the liquid valve.

The system was charged to a specific submergence ratio (H/L) while air was injected at a set flow rate. Since the flow was oscillatory, the system was run while the liquid flow rate was adjusted to keep the submergence ratio constant. Once the height of the fluid in the holding tank remained at a constant level, the system was considered to be at steady state and the liquid flow rate being fed back to the holding tank was recorded as the volumetric flow rate of fluid being pumped through the lift tube. Measurements were made for each of the three different lift tube diameters at each of the three submergence ratios for varying injected airflow rates.

The accuracy of the data is of course subject to the human error involved in reading the flow meters and the submergence level. To minimize errors, the experiments were repeated several times at each airflow rate to make sure that an accurate reading was taken. Upon repeating experiments, differences on the order of one half of a division of the flow meter scale were experienced between the measurements made; this corresponds to an average error of approximately 4% for the range of values tested.

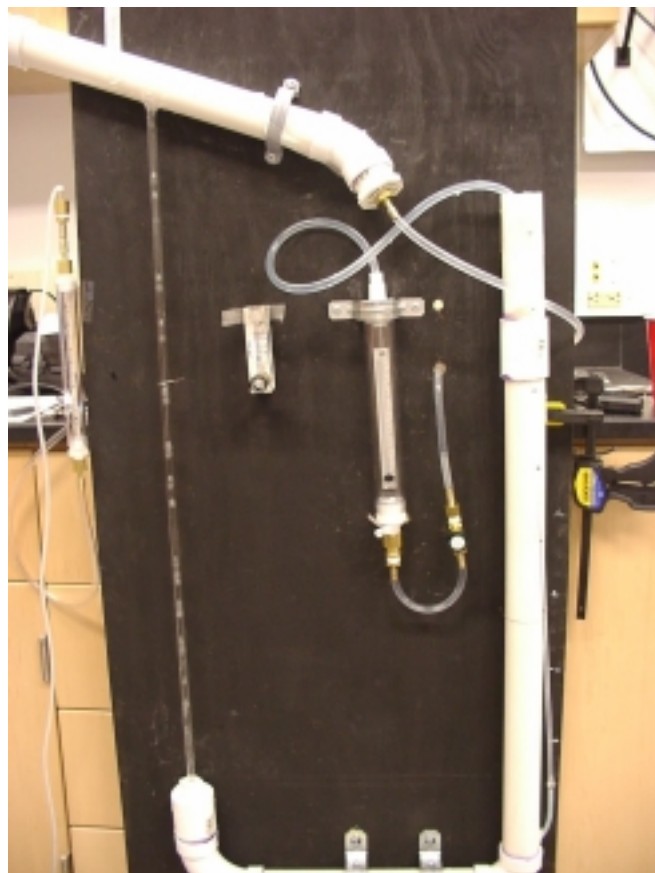


Figure 3.1: Experimental Setup

Experimental Results

Several flow patterns were observed in the experiments of the current study. At very low airflow rates bubbly flow was observed, but it did not pump the liquid up the tube at all. Upon slowly increasing the airflow rate, Taylor bubbles (bullet shaped bubbles which occupy almost the entire diameter) began to form and pushed the liquid up higher and higher until finally it was pumping the liquid out of the lift tube. This regime was slug flow, however it could also be considered slug/churn because it was quite intermittent. After increasing the airflow rate much further the flow transitioned to churn flow (also referred to as froth and semi-annular flow depending on the definition of these patterns), with the lift tube filling alternately with liquid and air. Finally at higher air flow rates a wispy annular/dispersed bubbly flow was observed, but this flow pattern was unstable, tending to transition back to churn flow under slight disturbances at any airflow rate.

It was found that the bubble pump operated most efficiently in the slug flow regime. Because of this, slug flow theories were used to model the bubble pump. However, the optimum operating zone was so close to the slug/churn transition, an equation for predicting this transition is necessary as a limiting value for a bubble pump design model.

CHAPTER IV

MODEL

Along with Delano's (1998) model, several empirical models from previous works are compared to the experimental data to see if they are valid in the range of diameters, submergence ratios, and lengths in the current study. For all models, the theoretical method of Stenning and Martin (1968) is used as the starting point to setup the relationship between the submergence ratio and the velocities (through momentum and mass balances). Additionally, each model (except for Delano who uses an empirical constant) uses the method of Beattie and Whalley (1982) to find the two-phase friction factor, and all but Delano uses the drift flux method (Zuber and Findlay 1965) to find the gas void fraction. The difference between these models is the value of the coefficients used in the drift flux model.

Governing Equations

The submergence ratio of the bubble pump, which describes the average pressure gradient along the lift tube, can be expressed in terms of velocities, geometrical parameters, and fluid properties by using momentum and mass balances. The following equations are based on Figure 2.1. Minor frictional losses in the entrance to the lift tube have been considered insignificant, while the change in momentum throughout the lift tube has also been neglected.

Momentum equation from P_{sys} to 0 gives:

$$P_0 = P_{sys} + \rho_L gH - \rho_L \frac{V_0^2}{2} \quad [4.1]$$

Where:

V_0 is the velocity (m/s) at point 0 (liquid solution)

Momentum equation from 0 to 1 yields (neglecting friction):

$$P_1 = P_0 - \rho_L V_0 (V_1 - V_0) \quad [4.2]$$

Where:

V_1 is the velocity (m/s) at state 1

D_0 is the diameter (m) of the water entrance line

L_0 is the length (m) of the water entrance line

Conservation of mass from state 0 to 1 yields:

$$\rho_L A_0 V_0 = \rho_L A_1 V_1 \quad [4.3]$$

Where:

Area of the water entrance line (m^2):

$$A_0 = \pi D_0^2 / 4 \quad [4.4]$$

Therefore:

$$V_0 = V_1 \quad [4.5]$$

Conservation of momentum from state 1 to 2, neglecting friction in this transition:

$$P_2 = P_1 - \rho_H V_1 (V_2 - V_1) \quad [4.6]$$

Where ρ_H is the homogeneous density of the two-phase flow. Since the velocities of each phase in the region between 1 and 2 are approximately equal (S=1) a homogeneous density is used in this momentum equation. This expression for the homogeneous density can be found from the conservation of mass from 1 to 2.

Conservation of mass from state 1 to 2 for the experimental air-lift pump setup yields:

$$\rho_L A_0 V_1 + m_G = \rho_H A_2 V_2 \quad [4.7]$$

Therefore:

$$\rho_H = \frac{\rho_L D_o^2 V_1 + \frac{4}{\pi} m_G}{D^2 V_2} \quad [4.8a]$$

For the ammonia-water bubble pump, the homogeneous density is obtained by eliminating the gas mass flow rate in Equation 4.8a:

$$\rho_H = \frac{\rho_L D_o^2 V_1}{D^2 V_2} \quad [4.8b]$$

At this point, the two-phase flow terminology from Chapter 2 is needed to proceed because the flow in the lift tube is most clearly defined in these terms. The

definitions of superficial velocities and void fraction can be related to the terminology used thus far.

Since states 0 and 1 are under liquid conditions:

$$V_0 = V_1 = \frac{Q_L}{A_0} \quad [4.9]$$

While the definition of j_L is:

$$j_L = \frac{Q_L}{A} \quad [2.6]$$

Therefore:

$$V_0 = V_1 = j_L \left(\frac{A}{A_0} \right) \quad [4.10]$$

Additionally, state 2 has two phases, but V_2 still describes the total average velocity of the mixture:

$$V_2 = \frac{Q_L + Q_G}{A} = \frac{Q}{A} \quad [4.11]$$

This is precisely the definition of j . Therefore:

$$V_2 = j \quad [4.12]$$

It follows from equations [4.10] and [4.12] that:

$$V_2 - V_1 = j - j_L \left(\frac{A}{A_0} \right) \quad [4.13]$$

Also, the void fraction is defined as the average cross sectional area occupied by the gas divided by the total cross sectional area of the pipe.

Therefore:

$$\frac{A_L}{A} = \frac{A - A_G}{A} = 1 - \varepsilon \quad [4.14]$$

Now the momentum equation in the lift tube (from state 2 to P_{sys}) can be stated as:

$$P_2 = P_{sys} + f_{TP} \frac{(\rho_L j_L + \rho_G j_G)^2}{2\rho_{TP}} \left(\frac{L}{D} \right) + \rho_L L g (1 - \varepsilon) \quad [4.15]$$

where f_{TP} is the two-phase friction factor, based on average properties of liquid and gas and ρ_{TP} is the two-phase density of the fluid mixture in the lift tube. Here, for the frictional pressure drop term, a two-phase density is required instead of a homogeneous one since there is now slip between the two phases. This two-phase density can be found from the density definition applied to the lift tube volume:

$$\rho_{TP} = \rho_G \varepsilon + \rho_L (1 - \varepsilon) \quad [4.16]$$

Therefore, combining Equations [4.1], [4.2], [4.5], [4.6] and [4.15], a general equation for the submergence ratio (H/L), which describes the average pressure gradient along the lift tube, can be solved as:

$$\frac{H}{L} = \frac{f_{TP}(\rho_L j_L + \rho_G j_G)^2}{2gD\rho_L\rho_{TP}} + \frac{j_L^2\left(\frac{D}{D_0}\right)^4}{2gL} + \frac{j_L\rho_H\left(\frac{D}{D_0}\right)^2\left(j - j_L\left(\frac{D}{D_0}\right)^2\right)}{\rho_L gL} + (1 - \varepsilon) \quad [4.17]$$

This equation is then used to model the flow in the bubble pump.

Two-Phase Properties

One issue in modeling two-phase flow is in predicting two-phase friction factors and properties of the mixture. These are needed in the governing equations. Lockhart and Martinelli (1949) defined a two-phase multiplier, used with a single-phase pressure drop calculation. While Beattie and Whalley (1982) recommend using the Colebrook equation for friction using two-phase properties in the Reynolds number derived from a homogeneous model, which models the single phase flow at the average properties of the individual phases.

$$\frac{1}{\sqrt{f'_{TP}}} = 3.48 - 4 \log_{10} \left[2 \frac{\varepsilon_R}{D} + \frac{9.35}{\text{Re}_{TP} \sqrt{f'_{TP}}} \right] \quad [4.18]$$

Where the parameters are defined as follows:

Fanning friction factor:

$$f'_{TP} = f_{TP} / 4 \quad [4.19]$$

Pipe roughness (m):

$$\varepsilon_R$$

Two-phase Reynolds number:

$$Re_{TP} = \frac{(\rho_G j_G + \rho_L j_L) D}{\mu_{TP}} \quad [4.20]$$

Two-phase viscosity (kg/m-s):

$$\mu_{TP} = \varepsilon_h \mu_G + \mu_L (1 - \varepsilon_h) (1 + 2.5 \varepsilon_h) \quad [4.21]$$

Homogeneous void fraction (when S =1):

$$\varepsilon_h = \frac{x}{x + \frac{\rho_L}{\rho_G} (1 - x)} \quad [4.22]$$

The Drift Flux Model

The drift flux model is now the widely accepted method for analyzing void fractions in two-phase flow. This method, formalized by Zuber and Findlay in 1965, provides a means to account for the effects of the local relative velocity between the phases as well as the effects of non-uniform phase velocity and concentration distributions.

While many others contributed to the beginnings of two-phase flow theory, Zuber and Findlay's (1965) analysis establishes the basis of the drift flux formulation used today (Chexal 1997). It relates the average gas void fraction of the two-phase flow to: 1) the superficial velocities (the velocity each phase would have if they occupied the entire area of the pipe alone) of the gas and liquid phases; 2) C_o , the distribution parameter; and 3) V_{gj} ($= V_G - j$), the drift velocity. The resulting drift flux model can be summarized by the following equation:

$$\varepsilon = \frac{j_G}{C_o(j_L + j_G) + V_{gj}} \quad [4.23]$$

Many authors have formulated empirical correlations for C_o and V_{gj} depending on the two-phase vertical flow regimes shown in Figure 2.2 and other parametric effects. In the current study, four models were examined which used different values of C_o and V_{gj} in the drift flux model to describe vertical two-phase flow. Since it was found that the bubble pump operated most efficiently in the slug regime, three of these models are

meant for slug flow only (Nicklin et al 1962, de Cachard and Delhay 1996, and Reinemann et al 1990). The fourth model (Chexal & Lellouche 1996) is not flow regime specific.

Nicklin Correlation

In 1962, Nicklin et al formulated an equation for the average velocity of the liquid slug (the entire denominator term in the drift flux model) in slug flow based on the work of Dumitrescu (1943) and Davies and Taylor (1950). The equation formulated by Nicklin et al has been so widely used to describe slug flow that is often considered the original slug flow model. Therefore, using the terminology from Equation 4.23, the first model examined uses:

$$C_0 = 1.2 \quad [4.24]$$

$$V_{gj} = 0.35 \sqrt{\frac{g(\rho_L - \rho_G)D}{\rho_L}} \approx 0.35 \sqrt{gD} \quad [4.25]$$

de Cachard & Delhay Correlation

Since the diameters in the current study were smaller than those previously used by authors who applied the Nicklin (1962) correlation to airlift analyses (Nicklin 1963; Clark & Dabolt 1986), surface tension effects may also be a consideration. de Cachard and Delhay (1996) took surface tension effects into account and came up with alternative empirical correlations for the V_{gj} term, still using $C_0 = 1.2$:

$$V_{gj} = 0.345 \left(1 - e^{-0.01N_f/0.345} \right) \left[1 - e^{(3.37-Bo)/m} \right] \sqrt{gD} \quad [4.26]$$

Where:

$$(N_f)^2 = \frac{\rho_L (\rho_L - \rho_G) g D^3}{\mu_L^2} \quad [4.27]$$

Bond number:

$$Bo = \frac{(\rho_L - \rho_G) g D^2}{\sigma} \quad [4.28]$$

And m is defined for different ranges of N_f :

$N_f > 250$:

$$m = 10 \quad [4.29a]$$

$18 < N_f < 250$:

$$m = 69(N_f)^{-0.35} \quad [4.29b]$$

$N_f < 18$:

$$m = 25 \quad [4.29c]$$

Reinemann Correlation

Reinemann et al (1990) also attempted to take into account surface tension effects by altering the V_{gj} term, with C_0 remaining as 1.2.

$$V_{gj} = 0.352 \left(1 - 3.18\Sigma - 14.77\Sigma^2 \right) \sqrt{gD} \quad [4.30]$$

Where:

Surface tension number:

$$\Sigma = \frac{\sigma}{\rho g D^2} \quad [4.31]$$

Chexal-Lellouche (CL) (1996) Correlation

Since the flow in the experiments was shown to transition to churn flow at high airflow rates, the previously mentioned slug flow models are not expected to observe this transition. Chexal and Lellouche (1996) devised an empirical program, which is derived from all the available experimental data in all flow regimes, in order to be able to use one model for all regimes. The equations for the distribution parameter and the drift velocity are much more complicated in this case:

Distribution Parameter:

$$C_0 = \frac{L_C}{K_0 + (1 - K_0)\epsilon^r} \quad [4.32]$$

Chexal-Lellouche fluid parameter, L_C , varies for different fluids:

For refrigerant mixtures :

$$L_C = \epsilon^{0.025(1+10\epsilon)} \exp[0.5(1 - \epsilon)] \quad [4.33a]$$

For air-water:

$$L_C = \min (1.15 * \epsilon^{0.45}, 1) \quad [4.33b]$$

Correlating fitting parameter :

$$K_0 = B_1 + (1 - B_1) \left(\frac{\rho_G}{\rho_L} \right)^{1/4} \quad [4.34]$$

Correlating fitting parameter :

$$r = \frac{1 + 1.57 \left(\frac{\rho_G}{\rho_L} \right)}{1 - B_1} \quad [4.35]$$

Where:

$$B_1 = \min(0.8, A_1) \quad [4.36]$$

$$A_1 = \frac{1}{1 + \exp\left(\frac{-\text{Re}_v}{60,000}\right)} \quad [4.37]$$

Re_v varies with Re_G and Re_L :

For $\text{Re}_G > \text{Re}_L$:

$$\text{Re}_v = \text{Re}_G \quad [4.38a]$$

For $\text{Re}_G \leq \text{Re}_L$:

$$\text{Re}_v = \text{Re}_L \quad [4.38b]$$

Drift Velocity (m/s) :

$$V_{gj} = 1.41 \left[\frac{(\rho_L - \rho_G) \sigma g}{\rho_L^2} \right]^{1/4} C_1 C_2 C_3 C_4 \quad [4.39]$$

Where:

$$C_1 = (1 - \varepsilon)^{C_{1v}} \quad [4.40]$$

$$C_{1v} = B_1 \quad [4.41]$$

C_2 varies with the liquid to gas density ratio:

For $\frac{\rho_L}{\rho_G} \leq 18$:

$$C_2 = 0.4757 \left[\ln \frac{\rho_L}{\rho_G} \right]^{0.7} \quad [4.42a]$$

For $\frac{\rho_L}{\rho_G} > 18$:

If $C_5 \geq 1$:

$$C_2 = 1 \quad [4.42b]$$

Else:

$$C_2 = 1 - \exp \left[\frac{-C_5}{1 - C_5} \right]$$

Where:

$$C_5 = \sqrt{\frac{150}{\frac{\rho_L}{\rho_G}}} \quad [4.43]$$

$$C_3 = \max \left(.5, 2 \exp \left(\frac{-\text{Re}_L}{300,000} \right) \right) \quad [4.44]$$

If $C_7 < 1$:

$$C_4 = \frac{1}{1 - \exp(-C_8)} \quad [4.45a]$$

Else:

$$C_4 = 1 \quad [4.45b]$$

Where:

$$C_7 = \left(\frac{D_2}{D} \right)^{0.6} \quad [4.46]$$

$$C_8 = \frac{C_7}{1 - C_7} \quad [4.47]$$

$$D_2 = .09144 \text{ m (reference diameter)} \quad [4.48]$$

Delano Correlation

Finally, the model of Delano (1998) uses the analysis of Stenning and Martin (1968). Instead of using the drift flux model to find the void fraction, Delano assigned a value to the slip, S, which is related to the void fraction by the following equation:

$$\varepsilon = \frac{1}{1 + S \cdot \frac{j_L}{j_G}} \quad [4.49]$$

The value for S was recommended by Stenning and Martin (1968) to be between 1.5 and 2.5 for optimum performance in the slug flow regime. Delano (1998) and Schaefer (2000) used 2.5. Additionally, Delano used an experimentally determined constant, K=17, which defines the friction factor correlation.

$$K = \frac{4fL}{D} = 17 \quad [4.50]$$

Delano's method is based on a slightly more simplified experimental setup than the current study's, but these differences have been neglected. The basis of this model is similar to equation 4.17, however the notation used by Delano is different.

$$\frac{H}{L} = \frac{1}{1 + \left[\frac{\dot{V}_G}{\dot{V}_L} \cdot \frac{1}{S} \right]} + \frac{j_L^2}{2gL} \left[K \left(1 + \frac{\dot{V}_G}{\dot{V}_L} \right)^2 + 2 \frac{\dot{V}_G}{\dot{V}_L} + 1 \right] \quad [4.51]$$

These variables were defined previously in Table 2.1.

Comparison of Models

These five different models were compared with the experiments to find the best candidate for modeling the bubble pump so that an optimum performance level can be predicted. Each model was programmed in EES (Engineering Equation Solver) (Klein and Alvarado 2000). For comparison, the system temperature and pressure used in each model were $T = 298 \text{ K}$, and $P = 1 \text{ bar}$, and the length of the lift tube was 3 ft. Air and water properties were taken from EES. As can be seen from figures 4.1-4.9, no single model works for the entire range of submergence ratios and diameters tested.

Most of the models used were not built to predict and account for the transition from slug to churn flow (the sharp increase in slope seen in the experimental data, for example, in Figure 4.1), but since the optimum performance occurs in the slug regime with a separate equation used to predict the transition (explained in detail in the next chapter), this was not considered a problem. However, it should be noted that the Chexal-Lellouche (1997) model does show a curve that could indicate a transition but it is at a much higher air and liquid flow rate than the experimentally observed transition (see, for example, Figure 4.1). Otherwise, the Chexal-Lellouche model seems to over

predict the airflow rate required to pump the liquid except at high submergence ratios (see Figures 4.1-4.6).

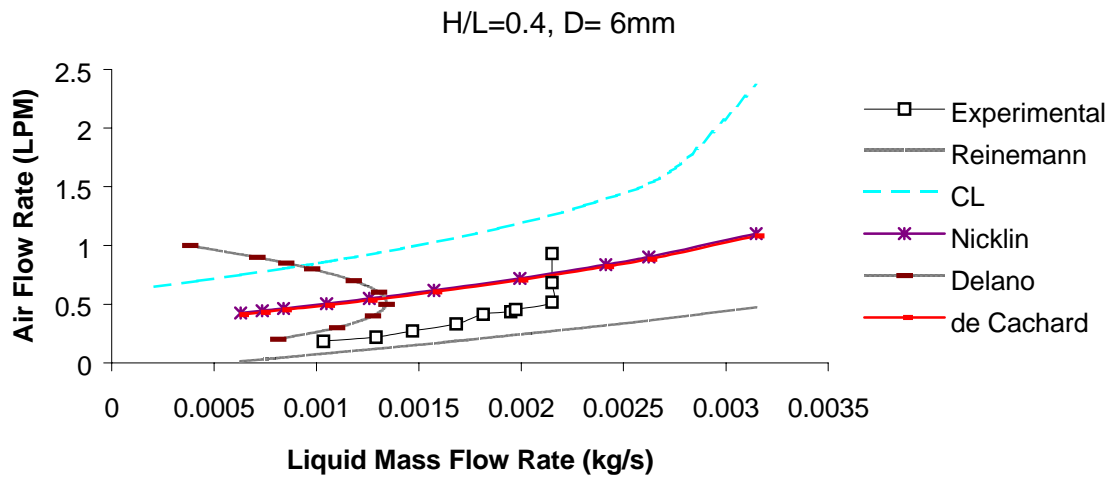


Figure 4.1: Air Flow Rate vs. Liquid Mass Flow Rate

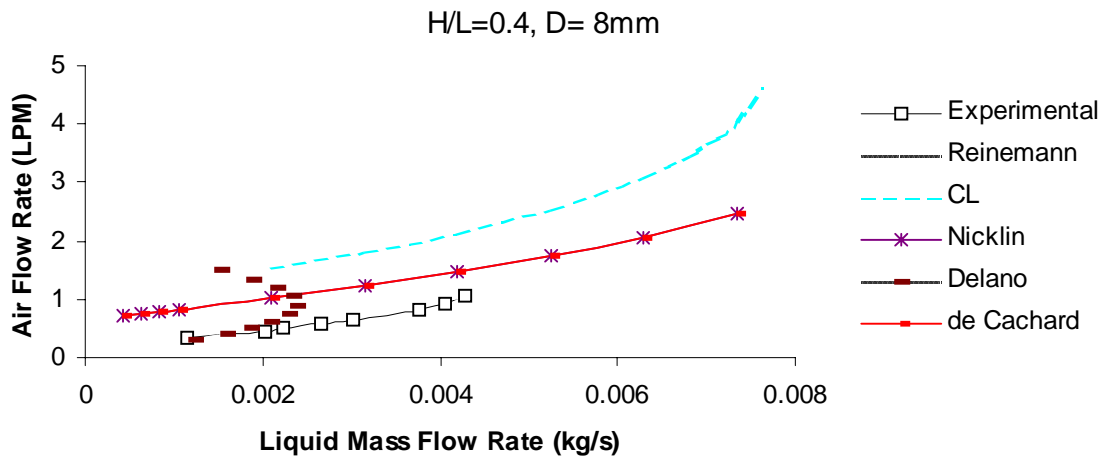


Figure 4.2: Air Flow Rate vs. Liquid Mass Flow Rate

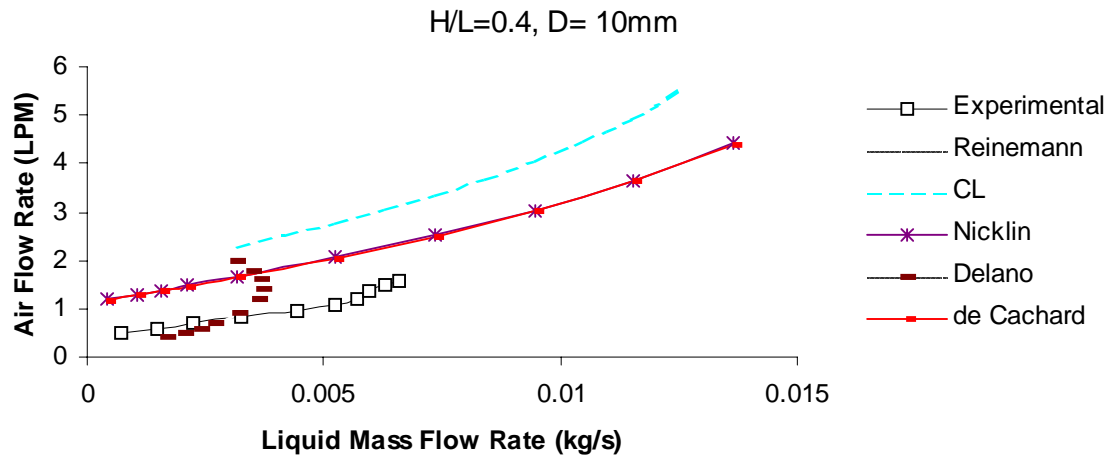


Figure 4.3: Air Flow Rate vs. Liquid Mass Flow Rate

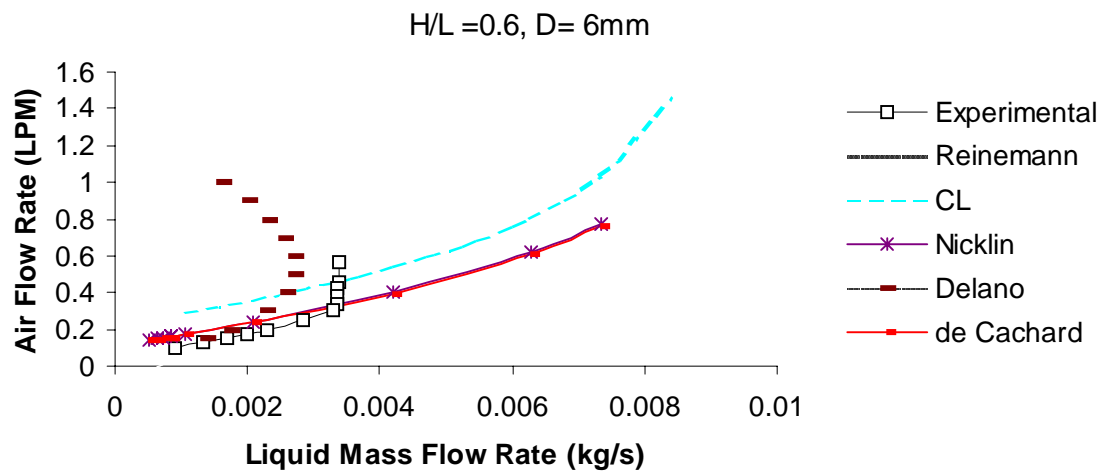


Figure 4.4: Air Flow Rate vs. Liquid Mass Flow Rate

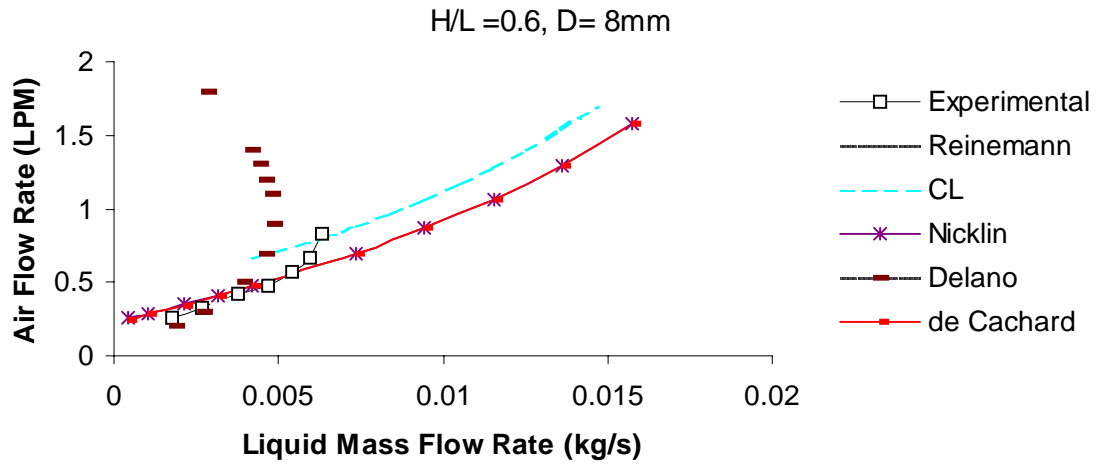


Figure 4.5: Air Flow Rate vs. Liquid Mass Flow Rate

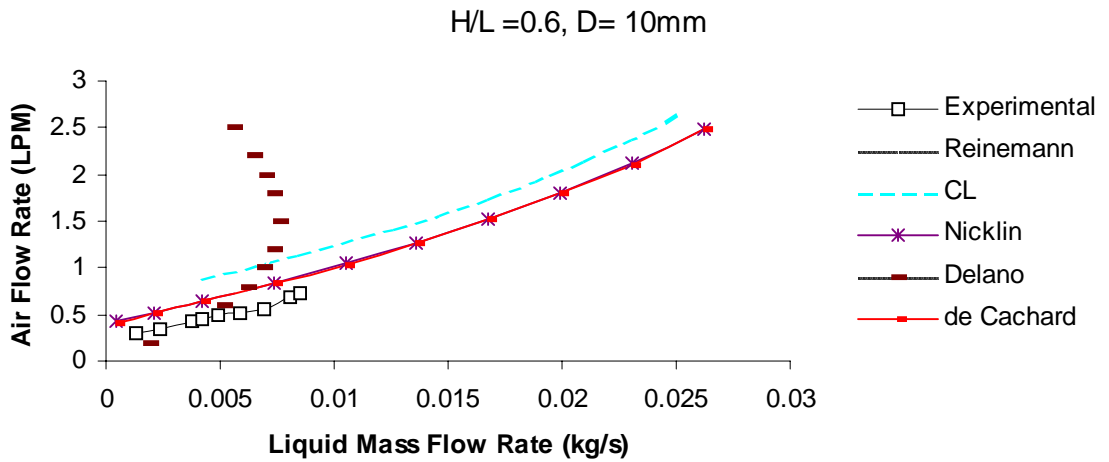


Figure 4.6: Air Flow Rate vs. Liquid Mass Flow Rate

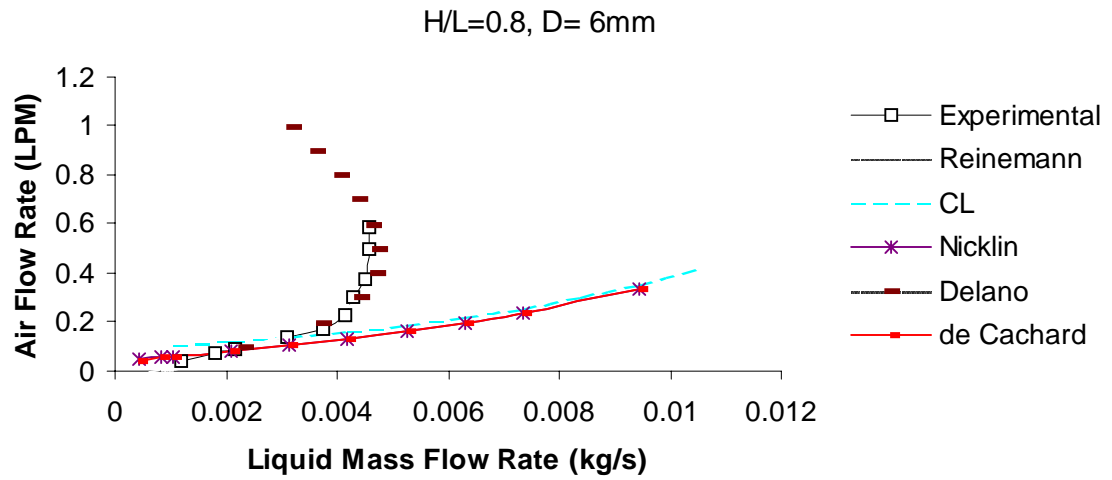


Figure 4.7: Air Flow Rate vs. Liquid Mass Flow Rate

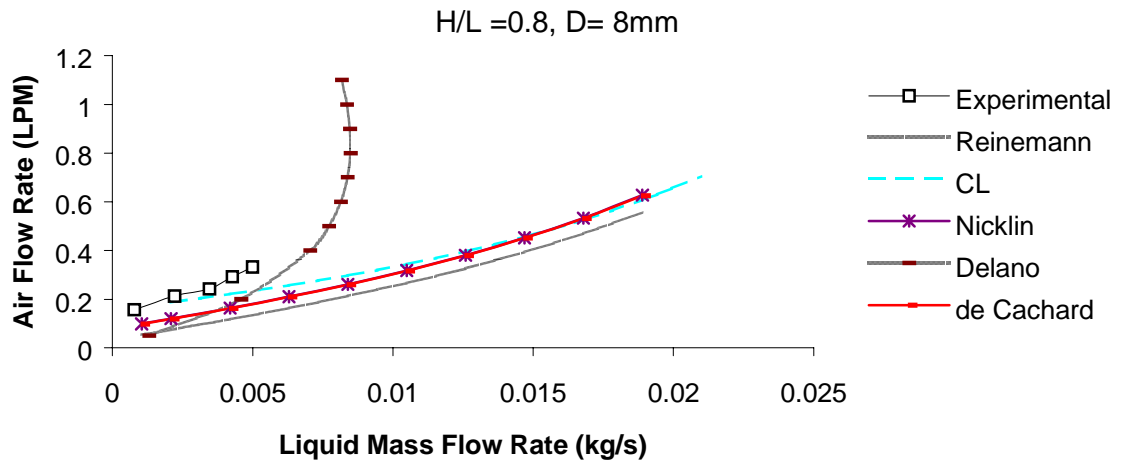


Figure: 4.8 Air Flow Rate vs. Liquid Mass Flow Rate

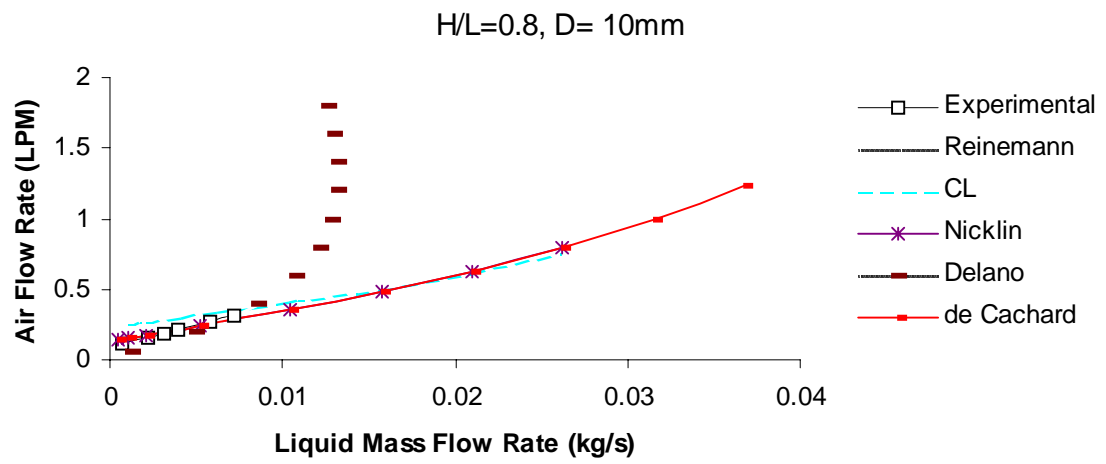


Figure 4.9: Air Flow Rate vs. Liquid Mass Flow Rate

Delano's (1998) model seems to have a noticeably different behavior than the other models (see figures 4.1-4.9), however, if the data for the other models had been extended into much higher flow rates, the same arched curve would be apparent for their plots in the figures as well. Therefore, even though Delano's model matches some of the experimental data pretty well (see figures 4.7-4.9), it is not capable of predicting the full range of slug flow data since it peaks out well before the experimental data transitions for lower submergence ratios.

Reinemann's (1990) model seems to work well at the lowest submergence ratio (Figures 4.1-4.3), however there is a problem with it at the smallest diameter for all submergence ratios (Figures 4.1, 4.4, and 4.7). In this model, the airflow rate goes to zero quicker than the liquid flow rate, causing a convergence problem at small diameters. Because of this inconsistency, this model has been thrown out of consideration.

The Nicklin et al (1962) and de Cachard & Delhaye (1996) models were almost identical for each case. They were also consistently the same slope as the experimental slug flow data, and not too far off of the values either. It mostly lacked in accuracy at the lowest alpha (see Figures 4.1-4.3). Because there were no anomalies with these models and they were reasonably close to the experimental data, these two models were prime candidates to be used to further analyze the optimization of the bubble pump. The de Cachard and Delhaye (1996) model was chosen because its values were slightly closer to the experimental ones. Therefore, from this point on the discussion of the model will refer to the one using the de Cachard and Delhaye correlation (Equations 4.26-4.29) for

the distribution parameter in the drift flux model (Equation 4.23), along with Equation 4.17 for the submergence ratio.

CHAPTER V

RESULTS AND DISCUSSION

Air-Lift Pump Experiments

From both the experimental and theoretical results (Figures 5.1-5.6) it can be seen that there is an optimum efficiency to operate the bubble pump for a given situation. For the air-lift pump analysis, efficiency is defined as the mass flow rate of liquid pumped in kg/s divided by the mass flow rate of air injected in kg/s. This efficiency is not on a typical 0 to 100 % scale; instead it is just a representation of the ratio of desired output to the required input for the bubble pump. When this ratio is maximized, the bubble pump operates most efficiently, hence the terminology. The important parameters that go into determining this optimum value, such as submergence ratio, diameter, length, and flow transition, are discussed here.

Parametric Studies

The most important parameter is the submergence ratio. As can be seen from Figures 5.1 to 5.6, the efficiency range is drastically larger for higher values of H/L. This makes sense, since if the submergence ratio were increased to one, no air flow would be needed to increase the buoyancy of the liquid, since the fluid would be able to reach the top of the lift tube by its own weight acting down in the generator. Therefore the mass flow rate of air would be zero, causing the efficiency to go to infinity. Hence, for any

design, to obtain the highest efficiency, the submergence ratio should always be maximized.

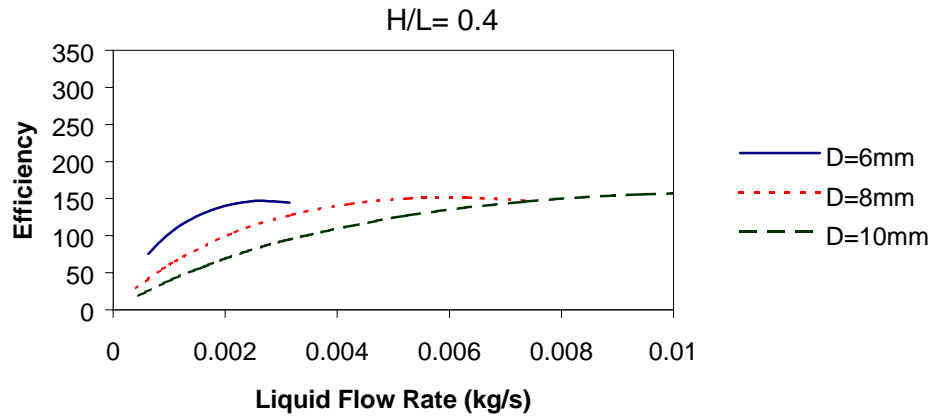


Figure 5.1: Theoretical Efficiency vs. Liquid Mass Flow Rate

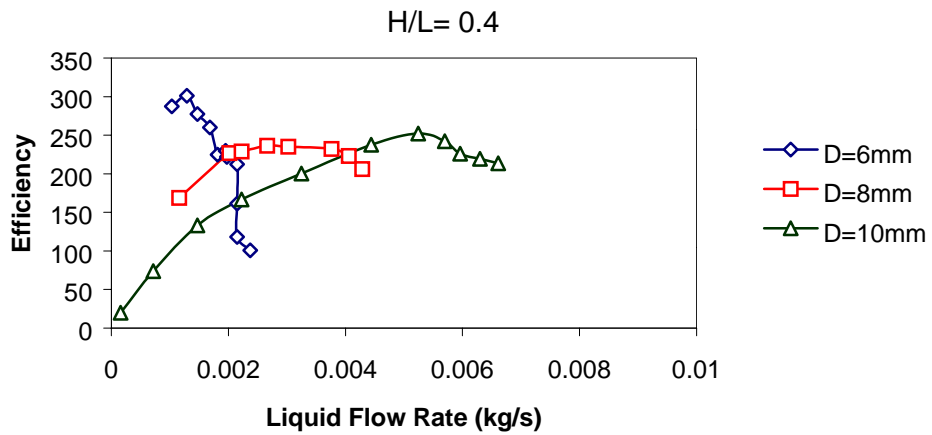


Figure 5.2: Experimental Efficiency vs. Liquid Mass Flow Rate

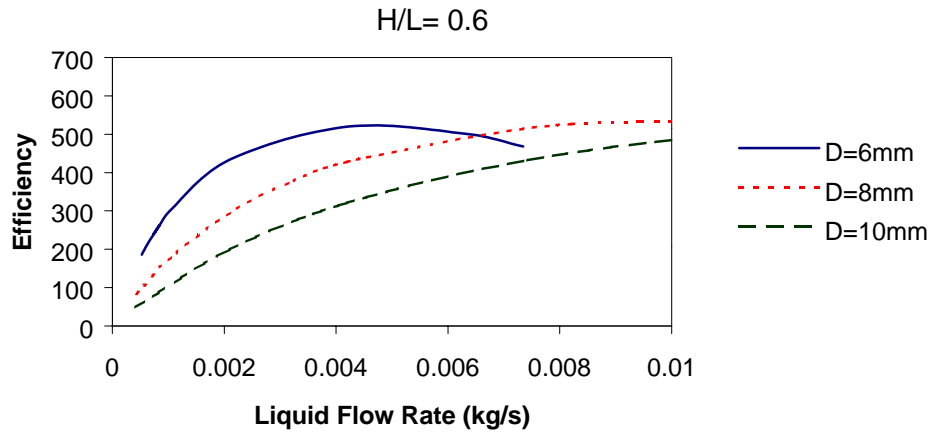


Figure 5.3: Theoretical Efficiency vs. Liquid Mass Flow Rate

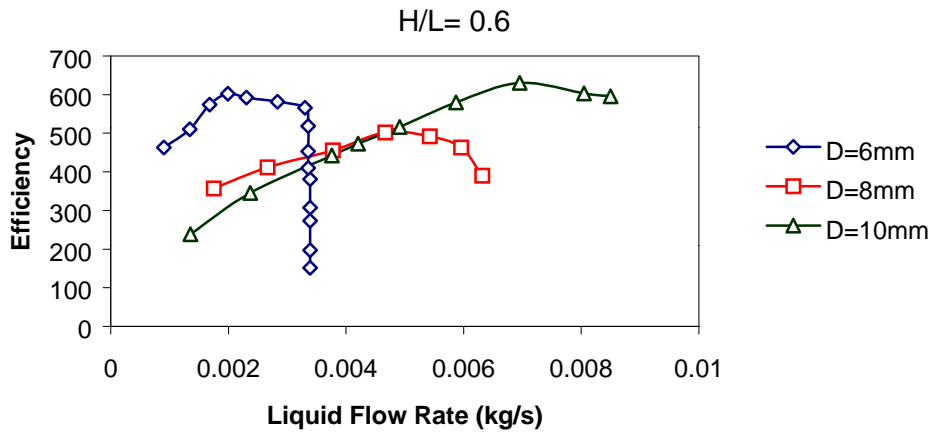


Figure 5.4: Experimental Efficiency vs. Liquid Mass Flow Rate

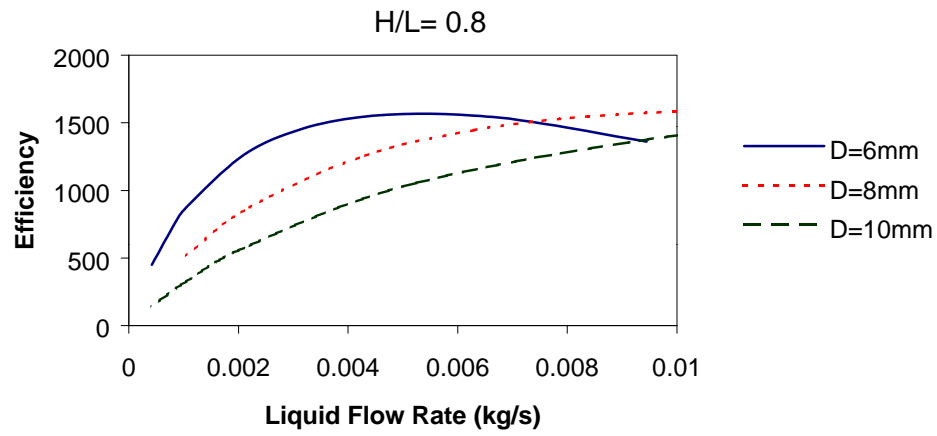


Figure 5.5: Theoretical Efficiency vs. Liquid Mass Flow Rate

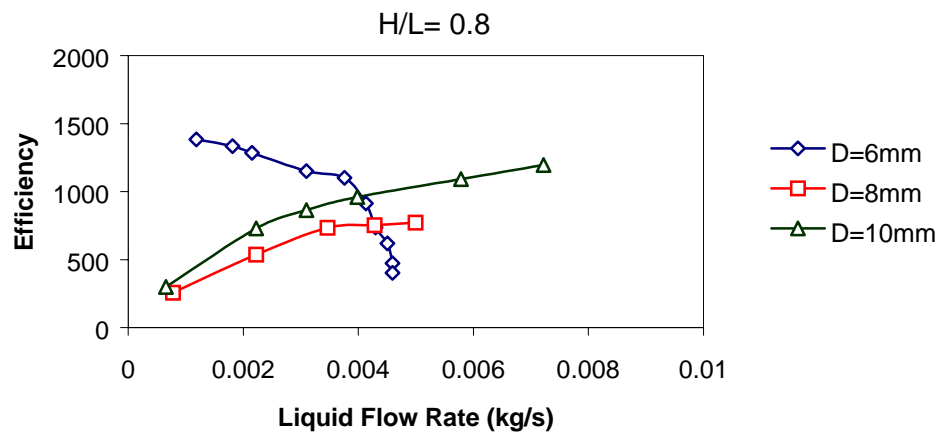


Figure 5.6: Experimental Efficiency vs. Liquid Mass Flow Rate

It was found from the experiments that the model is much more accurate for higher submergence ratios. Looking at figures 5.1 and 5.2 it can be seen that the efficiency predicted is less than that actually achieved for a submergence ratio of 0.4. de Cachard and Delhaye (1996) did not intend for this model to work at submergence ratios this low due to the occurrence of random oscillations which are difficult to model. From the experiments it is shown that these oscillations actually increase the efficiency of the pump.

Additionally, looking at Figures 5.1-5.6, a much higher efficiency was obtained for the 6 mm tube in the experimental studies than the model predicts. This is most likely due to the increased importance of surface tension as a parameter in small diameter tubes, which does not seem to be properly accounted for in the model.

Experiments were performed on 6 mm inner diameter tubes with lengths of 3 ft and 6 ft in order to determine the effect of length on the bubble pump operation. It was found that the bubble pump was not sensitive to the length of the tube, as seen for example in Figures 5.7 and 5.8. The location of transition from slug to churn flow, marked by a sharp change in slope, was at approximately the same liquid and airflow rates for both lengths as well.

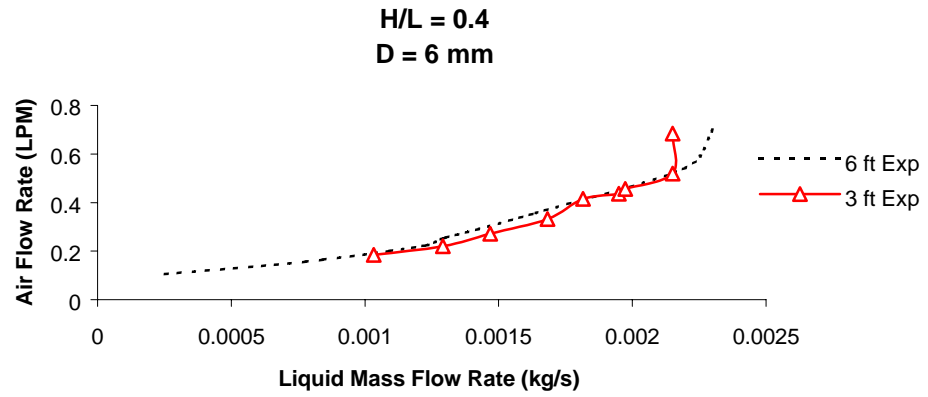


Figure 5.7: Length Effect: Experimental Airflow Rate vs. Liquid Mass Flow Rate

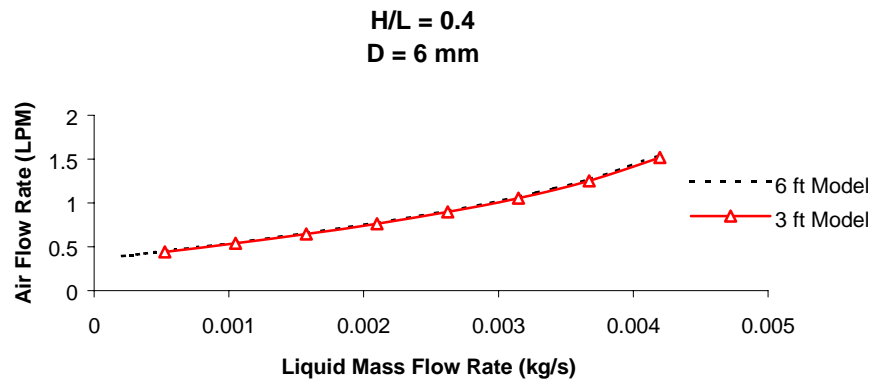


Figure 5.8: Length Effect: Theoretical Air Flow Rate vs. Liquid Mass Flow Rate

Optimum Operating Conditions

From Figures 5.1-5.6 it can be seen that there is an optimum efficiency to operate at for a specific diameter and submergence ratio. Operation at the peak of the curve would give the highest efficiency for a specific design scenario. It just so happens that the peak of the curve is very close to the transition from slug to churn flow. An example of this transition is seen in the sharp increase in slope in the experimental data of Figure 5.10 (all experimental plots were shown in Figures 4.1-4.9). Comparing this with the maximum point in Figure 5.9 it can be seen that the peak of the efficiency curve is very close to the transition from slug to churn flow, in fact it is right before the transition to churn, while once in the churn regime the efficiency decreases rapidly.

To make sure that the phenomena occurring was a transition from slug to churn flow, the experimental data was plotted on the Hewitt & Roberts Flow Map (1969) seen in Figures 5.10-5.12. While this plot is approximate, it can be seen that the flow experienced in the bubble pump is near the slug-churn transition. Therefore, since the de Cachard & Delhay (1996) model does not predict the transition, as an additional aide in finding the optimum operating conditions for any situation a transition criteria must be used as a limiting factor.

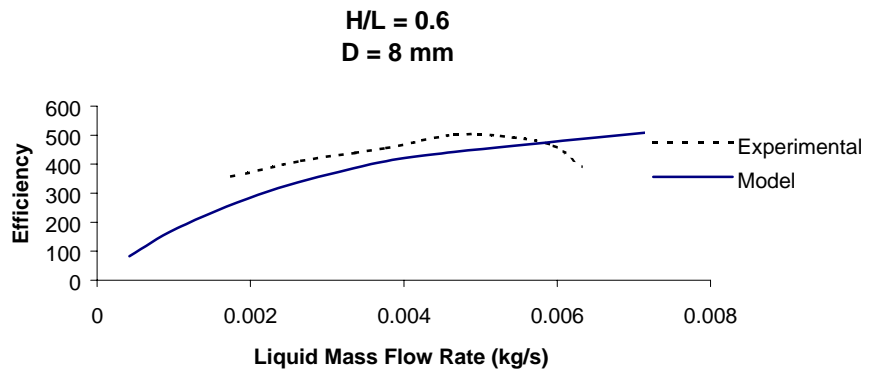


Figure 5.9: Efficiency vs. Liquid Mass Flow Rate

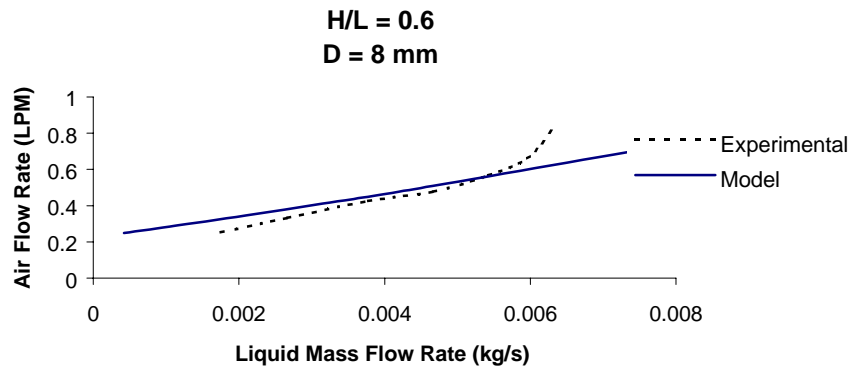


Figure 5.10: Air Flow Rate vs. Liquid Mass Flow Rate

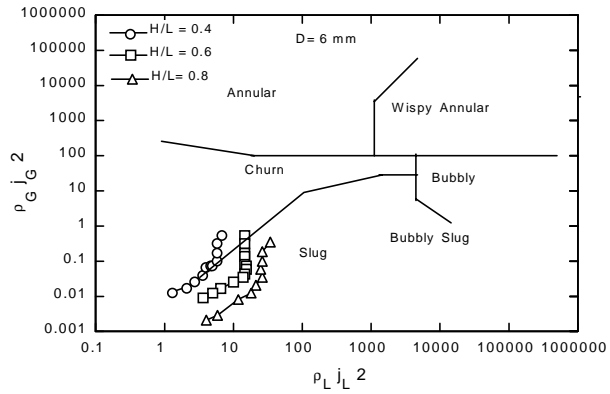


Figure 5.11: Flow Regime Map, $D=6\text{mm}$

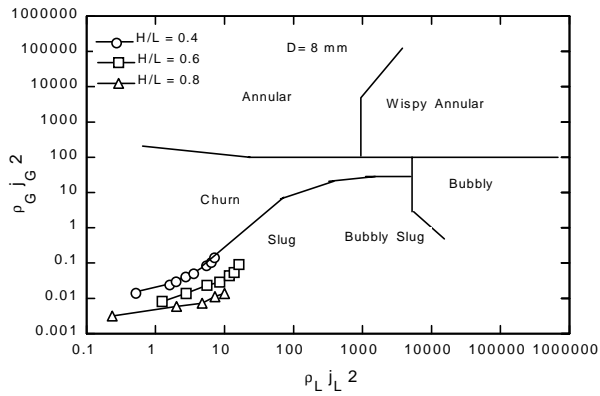


Figure 5.12: Flow Regime Map, $D=8\text{mm}$

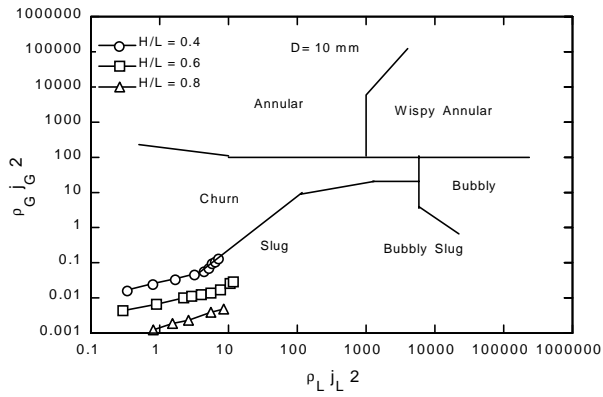


Figure 5.13: Flow Regime Map, $D=10\text{mm}$

Slug - Churn Transition

Jayanti and Hewitt (1992) reviewed four models for predicting the transition from slug to churn flow in vertical tubes. They concluded that the slug to churn transition is attributed to the flooding of the liquid film surrounding the Taylor bubble in slug flow. McQuillan & Whalley (1985), Nicklin & Davidson (1962), Wallis (1969), and Govan et al (1991) also came to this conclusion. Flooding is a phenomenon in which the liquid film in countercurrent flow of gas and liquid breaks down due to the formation of large interfacial waves (Jayanti and Hewitt 1992).

One method for the prediction of the flooding velocity is the following semi-empirical equation proposed by Wallis (1961) and Hewitt & Wallis (1963):

$$\sqrt{j_G^*} + \sqrt{j_L^*} = \text{Constant} \quad [5.1]$$

Where j_G^* and j_L^* , the non-dimensionalized gas and liquid superficial velocities are defined as:

$$j_G^* = j_G \frac{\sqrt{\rho_G}}{\sqrt{gD(\rho_L - \rho_G)}} \quad \text{and} \quad j_L^* = j_L \frac{\sqrt{\rho_L}}{\sqrt{gD(\rho_L - \rho_G)}} \quad [5.2]$$

However, Jayanti and Hewitt concluded that this model does not account for the effect of length of the falling film on the flooding velocity. To correct this, they suggest using:

$$\sqrt{j_G^*} + m\sqrt{j_L^*} = \text{Constant} \quad [5.3]$$

Where:

For $\frac{L}{D} \leq 120$:

$$m = 0.1928 + 0.01089\left(\frac{L}{D}\right) - 3.754 \times 10^{-5}\left(\frac{L}{D}\right)^2 \quad [5.4]$$

For $\frac{L}{D} > 120$:

$$m = 0.96 \quad [5.5]$$

According to Jayanti & Hewitt (1992), the constant in Equation 5.3 is 0.75 for sharp flanges into the tube and 0.88 for rounded flanges and a value of unity fits the data for smooth inlet and outlet conditions given by Hewitt and Wallis (1963). In the current study, a value of approximately 0.83 proved to be a very good predictor of the slug-churn transition. Therefore the following limitation, Equation 5.6, should be used as a constraint of the slug flow bubble pump model, with the optimum operating condition occurring at or below the point where the right hand side value is approximately 0.83. Beyond this value, transition to churn flow diminishes the bubble pump's efficiency.

$$\sqrt{j_G^*} + m\sqrt{j_L^*} < 0.83 \quad [5.6]$$

Ammonia-Water Model

With the model verified by the experimental data of the air-water system, it was then used to analyze the design considerations of a bubble pump using an ammonia-water mixture, such as that needed in the Einstein cycle. In the case of a single pressure absorption refrigeration cycle the required liquid flow rate is a given constraint while the amount of heat added to the cycle to create enough vapor to pump this liquid is preferably minimized for maximum cycle efficiency. Therefore the variables that can be used to maximize the efficiency are geometrical, the submergence ratio and the diameter of the lift tube. For the ammonia-water model, efficiency was defined as the mass flow rate of liquid pumped in kg/s divided by the heat input in kW. Therefore, once again, this efficiency is not on a 0 to 100 % scale, but it is also has the units of kg/kJ.

The system temperature and pressure used for calculations were 375 K and 4 bars respectively, while the fluid used was an ammonia-water mixture of 15.5% ammonia concentration. These values were determined by the generator outlet conditions from Delano's (1998) base case design of the Einstein Cycle. Properties of the ammonia-water mixture other than surface tension and viscosity were found using the thermophysical property functions in EES. The surface tension of the ammonia-water mixture was found in IIR (1994) to be 0.043 N/m under the prescribed system pressure and concentration. The solution viscosity was also found in IIR (1994) to be approximately 0.0003 kg/m-s.

The submergence ratio and the mass flow rate of the liquid were varied to find their respective importance, while the length of the lift tube was set to 0.5 m.

Additionally, the diameter of the entrance line (D_0) was set equal to the diameter of the lift tube (D). Finally, the tube diameter was varied between about 4 mm and 40 mm depending on where the maximum efficiency was found for each case. Efficiency is defined as the liquid mass flow rate pumped per unit of heat input to the bubble pump (\dot{m}_L/\dot{Q}_{BP}). The efficiency was plotted versus the diameter to find the optimum lift tube diameter. The resulting plots are shown in Figures 5.14-5.16.

The liquid mass flow rates used in the program were again derived from the base case of Delano's (1998) design. His entire model was scaled to the mass flow rate in the bubble pump. Therefore an evaporator refrigerating capacity was chosen as 1000 W and the corresponding necessary flow rate was calculated:

$$\dot{Q}_{evap} = 1000 \frac{J}{s} = 3412 \frac{Btu}{h} \quad [5.7]$$

$$Q_{evap} = 133.4 \frac{kJ}{kg} \quad [5.8]$$

$$\dot{m}_L = \frac{\dot{Q}_{evap}}{Q_{evap}} = 0.0075 \frac{kg}{s} \quad [5.9]$$

In order to obtain a range of values, liquid mass flow rates of 0.0025 kg/s and 0.02 kg/s were also tested.

As mentioned in the air-water results, the most important parameter is the submergence ratio, and should always be maximized to obtain the highest efficiency, however there is also an optimum diameter for a specific liquid mass flow rate and submergence ratio, as seen in Figures 5.14-5.16. The location of the transition from slug

to churn flow, as predicted by Equation 5.6, is plotted in the figures as well. It can be seen that in many cases the transition to churn flow is well after the optimum value has been reached, but sometimes it is before the peak of the curve so the optimum is the last point on the curve at the cutoff point because beyond this point the model is not valid. Figure 5.17 summarizes the results showing the optimum efficiency diameter vs. liquid mass flow rate.

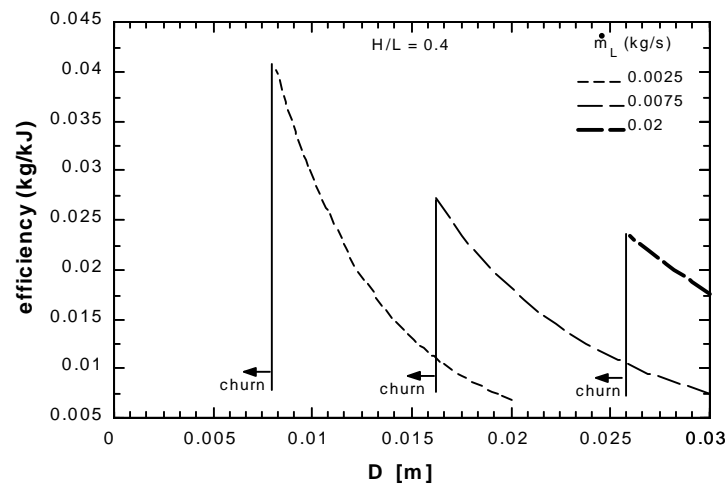


Figure 5.14: Efficiency vs. Diameter ($H/L = 0.4$)

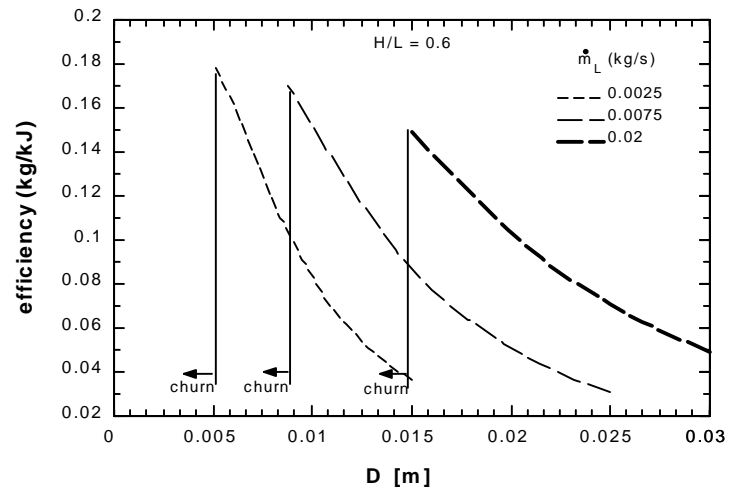


Figure 5.15: Efficiency vs. Diameter ($H/L = 0.6$)

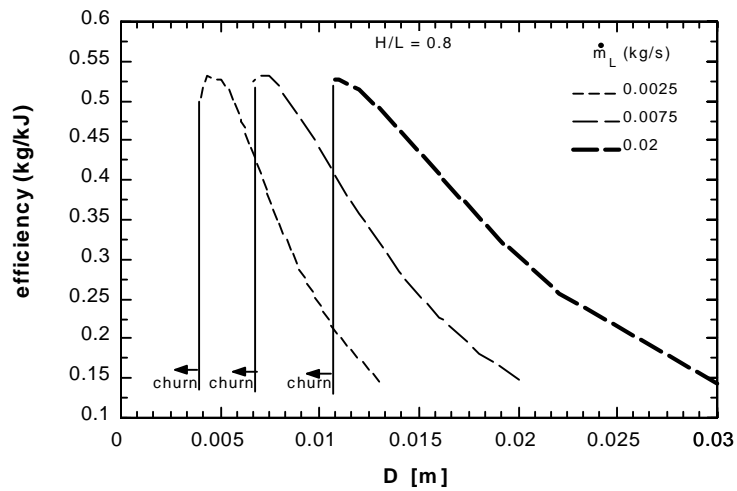


Figure 5.16: Efficiency vs. Diameter ($H/L = 0.8$)

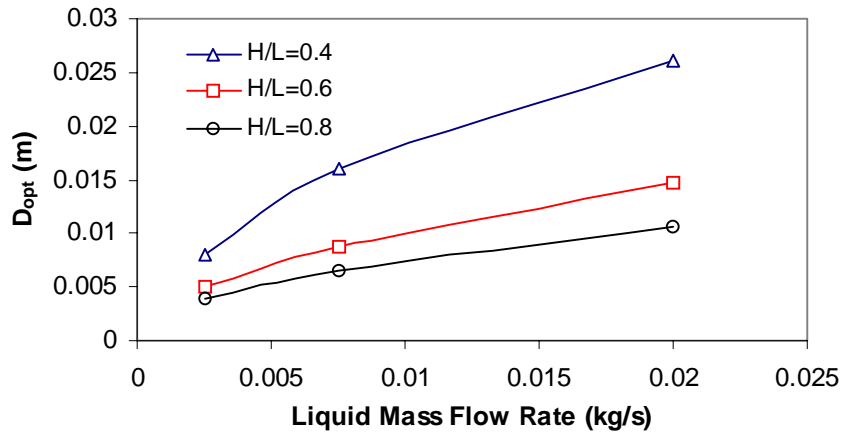


Figure 5.17: Optimum Efficiency Diameter vs. Liquid Mass Flow Rate

For comparison, Delano (1998) investigated a bubble pump with submergence ratios between 0.1 and 0.3. It was found using Equation 5.6 that with these H/L values over the applicable range of liquid mass flow rates, the flow would be entirely churn, even though Delano's (1998) model assumes slug flow conditions. Schaeffer (2000) has the same problem. By increasing the submergence ratio to 0.4, slug flow conditions are attainable. In Delano's study the Diameter was fixed, here the diameter was a parameter in designing for optimum efficiency.

From the experiments it is expected that diameters less than 6 mm will have higher efficiencies than those predicted by the model as well as situations with submergence ratios around 0.4. This may be due to the increased importance of surface tension at small diameters and the random oscillations at low submergence ratios,

respectively. While submergence ratios lower than 0.4 are likely to be in the churn regime over a large range of diameters.

CHAPTER VI

CONCLUSIONS AND RECOMMENDATIONS

One of the greatest benefits of single pressure absorption refrigeration cycles is that they do not need a mechanical input. Due to their low head requirement, they can utilize a thermally driven bubble pump instead of a compressor or solution pump. However, the thermal requirement of the bubble pump can be very significant compared to the generator, reducing the thermal efficiency of the single pressure absorption cycle. Therefore, this bubble pump heat input should be minimized.

The objective of the current study was to accurately model the bubble pump using two-phase flow correlations and find the optimum design parameters. Five different models were compared and it was verified through experiments with an air-water system that the drift flux based model by de Cachard and Delhaye (1996) was the closest fit to the data. From the experiments it was found that bubble pump operation is not sensitive to the length of the lift tube, however it is highly dependant on the submergence ratio. Additionally, it was found that there is an optimum condition for which to operate the pump. This optimum occurs in the slug regime near the slug-churn transition, therefore an equation for predicting this transition by Wallis (1961) and Hewitt & Wallis (1963) was used as a limiting factor for design.

The model was then used to analyze an ammonia-water system and it was found that there is an optimum diameter, ranging from 4 mm to 26 mm for a required liquid

pumping rate of 0.0025 kg/s to 0.02 kg/s, for maximizing the efficiency of the bubble pump component. However, the efficiency rapidly decreases when diameters smaller than the optimum value are used; therefore it is recommended to use a slightly larger diameter than the optimum value.

The peak efficiency values for the cases studied ranged from a low of about 0.025 kg/KJ for a required liquid flow of 0.02 kg/s and submergence ratio of 0.4, to a high of about 0.53 kg/KJ for all of the liquid flow rates and submergence ratio of 0.8. The optimum efficiency value is most sensitive to the submergence ratio, changing by a factor of about ten as the submergence changes from 0.4 to 0.8 at a fixed liquid flow rate. Changing the liquid flow rate at a fixed submergence ratio has a lesser effect especially at higher submergence ratio. At $H/L = 0.4$, the efficiency changes by about a factor of two as the flow rate is varied by a factor of three.

For fixed submergence ratio and liquid flow rate, there is a rapid drop in efficiency as the diameter drops below some value. This rapid drop off is due to the transition from slug to churn flow. Therefore, a limiting lower diameter value should be set to stay out of the churn flow regime and remain in the slug regime. If the calculated peak efficiency predicted by the two-phase model occurs in the churn regime, the bubble pump should be designed at a larger diameter, so that it operates in the slug flow regime. Equation 5.6 predicts this flow transition. If the right hand side is less than 0.83, then the flow will be in the slug flow regime.

It should be noted that this model is not expected to be very accurate below diameters of approximately 6 mm due to the increasing influence of surface tension in

that range which does not seem to be accounted for accurately in the current model. It is suggested that in future studies the surface tension effects at very small diameters be included in the analysis as well as the inconsistencies between the model and experiments at low submergence ratios.

REFERENCES

- Beattie, D.R.H., and Whalley, P.B. 1982. A simple two-phase frictional pressure drop calculation method. Int. J. of Multiphase Flow, Vol. 8, pp. 83-87.
- de Cachard, F. and Delhaye, J.M. 1996. A slug-churn model for small-diameter airlift pumps. Int. J. Multiphase Flow, Vol. 22, No. 4, pp. 627-649.
- Chen, J.; Kim, K.J.; Herold, K.E. 1996. Performance enhancement of a diffusion-absorption refrigerator. Int. J. Refrig. Vol. 19, No. 3, pp. 208-218.
- Chexal, B., Lellouche, G., Horowitz, J., and Healzer, J. 1992. A void fraction correlation for generalized applications. Progress in Nuclear Energy, Vol. 27, No. 4, pp. 255-295.
- Chexal, B.; Merilo, M.; Maulbetsch, M.; Horowitz, J.; Harrison, J.; Westacott, J.; Peterson, C.; Kastner, W.; and Schmidt, H. 1997. Void Fraction Technology for Design and Analysis. Electric Power Research Institute, Palo Alto, CA.
- Chisholm, D. 1983. Two-phase flow in pipelines and heat exchangers, George Goodwin, New York.
- Clark, N.N. and Dabolt, R.J. 1986. A general design equation for air lift pumps operating in slug flow. AIChE Journal, Vol. 32, No. 1, pp. 56-64.
- Collier, J.G., and Thome, J.R. 1996. Convective Boiling and Condensation. McGraw-Hill Book Co., New York.
- Davies, R.M. and Taylor, G.I. 1950. The Mechanics of large bubbles rising through extended liquids and through liquids in tubes. Proc. Roy. Soc. Vol. A200, pp. 357.
- Delano, A.D. 1998. Design Analysis of the Einstein Refrigeration Cycle, PhD Dissertation, Georgia Institute of Technology.
- Dumitrescu, D.T. 1943. Stromung an einer luftblase im senkrechten rohr. Z. Angew. Math. Mech. Vol. 23, pp. 139-149.

- Dorairaj, S. and Agarwal, R.S. 1987. Prediction of transport properties of R22-DMF refrigerant absorbent combinations. Int. J. Refrigeration, Vol. 10, July, pp.224-228.
- Einstein, A. and Szilard, L. 1930. Refrigeration. (Appl. U.S. Patent: 16 Dec. 1927; Priority: Germany, 16 Dec. 1926).
- Einstein, A. and Szilard, L. 1928. Improvements Relating to Refrigerating Apparatus. (Appl. U.K. Patent: 16 Dec. 1927; Priority: Germany, 16 Dec. 1926)
- Gibson, A.H. 1908. Hydraulic and its applications, Constable and Co. Publishers, London. pp. 192-200, 681-689.
- Govan, A.H.; Hewitt, G.F.; Richter, H.J. and Scott, A. 1991. Flooding and churn flow in vertical pipes. Int. J. Multiphase Flow. Vol. 17, pp. 27-44.
- Griffith, P. and Wallis, G. 1961. Two-phase slug flow. ASME Journal of Heat Transfer, Vol. 83, pp. 307-320.
- Hassoon, H. 1989. A two-phase investigation relating to circulating bubble absorbers. PhD thesis, Mechanical Engineering Department, University of Bristol, U.K.
- Herold, K.E.; Radermacher, R. and Klein, S.A. 1996. Absorption Chillers and Heat Pumps. CRC Press, Boca Raton, FL.
- Hewitt, G.F., and Roberts, D.N. 1969. Studies of two-phase flow patterns by simultaneous x-ray and flash photography. AERE-M 2159, HMSO.
- Hewitt, G.F. and Wallis, G.B. 1963. Flooding and associated phenomena in falling film flow in a vertical tube. UKAEA Report No. AERE-R4022. HMSO, London.
- IIR, 1994, Thermodynamic and Physical Properties of NH₃-H₂O, International Institute of Refrigeration.
- Jayanti, S. and Hewitt, G.F. 1992. Prediction of the slug-to-churn flow transition in vertical two-phase flow. Int. J. Multiphase Flow, Vol. 18, No. 6, pp. 847-860.
- Kendall, J. and Monroe, K.P. 1917. J. Am. Chem. Soc., Vol. 39, pp. 1802
- Kim, K.J.; Chen, J. and Herold, K.E. 1995. Hotel room air conditioner design based on a diffusion absorption cycle. ASHRAE Trans. Vol. 101, Part 1, pp. 1290-1301.
- Klein, S.A. and Alvarado, F.L. 2000. Engineering Equation Solver, F-Chart Software, Ver.6.036.

- Kouremenos, D.A. and Staicos, J. 1985. Performance of a small air-lift pump. Int. J. Heat Fluid Flow, Vol. 6, pp. 217-222.
- Lin, S.; Kwok, C.C.K.; Li, R.-Y.; Chen, Z.-H.; and Chen, Z.-Y. 1991. Local frictional pressure drop during vaporization of R-12 through capillary tubes. Int. J. Multiphase Flow, Vol. 17, pp. 95-102.
- Lockhart, R.W. and Martinelli, R.C. 1949. Proposed correlation of data for isothermal two-phase, two-component flow in pipes. Chem. Eng. Prog., Vol. 45, pp 39-48.
- McQuillan, K.W. and Whalley, P.B. 1985. Flow patterns in vertical two-phase flow. Int. J. Multiphase Flow. Vol. 11, pp. 161-175
- Nicklin, D.J. and Davidson, J.F. 1962. The onset of instability in two-phase slug flow. Presented at a Symp. on Two-phase flow, Inst. Mech. Engrs, London, paper No 4.
- Nicklin, D.J.; Wilkes, M.A. and Davidson, M.A. 1962. Two-phase flow in vertical tubes. Trans. Instn. Chem. Engrs., Vol. 40, pp. 61-68.
- Nicklin, D.J. 1963. The air-lift pump: theory and optimization. Trans. Instn. Chem. Engrs., Vol. 41, pp 29-39.
- Pickert, F. 1932. The theory of the air-lift pump. Engineering, Vol. 34, pp. 19-20.
- von Platen, B.C. and Munters, C.G., 1928. "Refrigerator", U.S. Patent 1,685,764.
- Reinemann, D.J., Parlange, J.Y., and Timmons, M.B. 1990. Theory of small-diameter airlift pumps. Int. J. Multiphase Flow, Vol. 16, pp. 113-122.
- Sathe, A. 2001. Experimental and theoretical studies on a bubble pump for a diffusion absorption refrigeration system. Master of Technology Project Report, Universitat Stuttgart. (<http://www.geocities.com/abhijitsathe/project/project.html>)
- Schaefer, L. A. 2000. Single Pressure Absorption Heat Pump Analysis, PhD Dissertation, Georgia Institute of Technology.
- Shelton, S.; Delano, A. and Schaefer, L. 1999. Second Law Study of the Einstein Refrigeration Cycle, Proceedings of the Renewable and Advanced Energy Systems for the 21st Century, April 1999.
- Stenning, A. and Martin, C. 1968. An analytical and experimental study of air-lift pump performance, ASME Journal of Engineering for Power pp. 106-110.

- Stepanoff, A.J. 1929. Thermodynamic theory of the air lift pump. ASME Transactions, Vol. 51, pp.49-55.
- Todoroki, I., Yoshifusa, S. and Honda, T. 1973. Performance of air-lift pump. Bulletin of ASME, Vol. 16, pp. 733-741.
- Wallis, G.B. 1961. Flooding velocities for air and water in vertical tubes. UKAEA Report No. AEEW-R123. HMSO, London.
- Wallis, G.B. 1969. One-dimensional Two-phase Flow. McGraw-Hill, New York.
- Watson, M.J. and Hewitt, G.F. 1999. Pressure effects on the slug to churn transition. Int. J. of Multiphase Flow, Vol 25, pp. 1225-1241.
- White, E.T. and Beardmore, R.H. 1962. The velocity of rise of single cylindrical air bubbles through liquids contained in vertical tubes. Chem. Engng Sci., Vol. 17, pp 351-361.
- Zuber, N. and Findlay, J. 1965. Average volumetric concentration in two-phase flow systems. J. of Heat Transfer, Vol. 87, pp. 453-468.
- Zukoski, E.E. 1966. Influence of viscosity, surface tension, and inclination angle on motion of long bubbles in closed tubes. J. Fluid Mech., Vol. 20, pp 821-832.